Intrathecal delivery of antisense oligonucleotide therapeutics: transport mechanisms and factors influencing distribution in the central nervous system

By
Brynna Wilken-Resman

A dissertation submitted in partial fulfillment of the requirement for the degree of

Doctor of Philosophy
(Pharmaceutical Sciences)

at the
University of Wisconsin-Madison
2019

Date of final oral examination: 02 December 2019

This dissertation is approved by the following members of the Final Oral Committee:
Charles T. Lauhon, Associate Professor, Pharmaceutical Sciences
Lingjun Li, Professor, Pharmaceutical Sciences
Michael R. Taylor, Assistant Professor, Pharmaceutical Sciences
Zsuzsanna Fabry, Professor, Pathology and Laboratory Medicine
Robert G. Thorne, PhD, Denali Therapeutics

© Copyright Brynna Wilken-Resman 2019
All Rights Reserved

Acknowledgements

There are many people within the University of Wisconsin-Madison community and beyond who have played a role in my scientific development. I'd first like to thank my advisor, Dr. Robert Thorne, for encouraging my scientific progress, for passing along his advice and enthusiasm for science, and for being an advocate for his students. I have greatly appreciated his guidance. Chapter 1 of my dissertation is dedicated to him as recognition that he has imparted the importance of understanding the history and background of the scientific field in which we have conducted this research. As a thesis committee member, Dr. Charles Lauhon has provided valuable insight for my research and as my co-advisor, he provided support, advocacy, and the ability to seamlessly continue my research which I am extremely grateful for. I would also like to thank the members of my thesis committee, who have contributed to my knowledge through coursework and helped guide my research: Dr. Michael Taylor, Dr. Zsuzsanna Fabry, and Dr. Lingjun Li.

I am deeply appreciative of the Thorne Lab members who became the friends that I was fortunate to spend my days with: Geetika Nehra, Michelle Pizzo, Niyanta Kumar, Dan Wolak, and Jeff Lochhead. Due to significant overlap in our research, Michelle spent countless hours training and mentoring me, and I appreciate her generosity and patience. I would also like to thank Tongzhen Xie and Gretchen Greene for their assistance and conversation, both science-related and otherwise. I am grateful for the support of friends who weren't in the lab but with whom I managed to spend a significant amount of time, occasionally under the pretense of working on coursework, including Mint and Kelly.

One of the most enjoyable parts of graduate school has been the connections made with other students in the Pharmaceutical Sciences program and beyond in the UW-Madison community, including in the classroom, AAPS, intramural sports, or passing by and stopping to talk in the hallways. I'd like to thank the graduate program coordinator Ken Niemeyer who has played a role far outside his job description. He is a reliable, positive presence in the department and routinely goes out of his way to improve the experience of graduate school for students.

My introduction and my initial draw to scientific research occurred during my undergraduate years at the University of Minnesota in the lab of Dr. Bill Elmquist. Dr. Elmquist provided me with opportunities that pushed me to stretch my knowledge and skills. Karen, Shruthi, Raj, and Rajneet were mentors with a high tolerance for my many questions who I thank for allowing me to "help" with their experiments as a beginner. I also learned a great deal and enjoyed spending time with Gautham, Janice, Minjee, Shuangling, and Sani during our time together in the lab.

Lastly, I want to thank my family for the support they have given me while I pursued educational and other goals. Throughout my life my parents, Steve and Cresy, have given me guidance on the value of education. They encouraged me to enjoy the times when pursuing a goal is fulfilling and to continue pursuing that goal despite any setbacks along the way. I'm fortunate to have an older brother, Eli, who is a built-in friend and supporter and who greatly influenced my decision to pursue a PhD. Finally, I want to thank my partner, Sam, for his constant support, including listening to numerous practice talks, reading scientific posters, and cushioning setbacks and celebrating achievements in graduate school and in life.

Abstract

Antisense oligonucleotide (ASO) therapies for central nervous system (CNS) indications have advanced significantly within the past three years, including FDA approval for an ASO therapy for spinal muscular atrophy and clinical trials for several other neurological disorders. ASOs are ~6-8 kDa, single-stranded DNA or RNA oligomers and are attractive therapeutic candidates for diseases caused by known genetic abnormalities because they are disease-modifying therapeutics that can interact with target RNA to modify protein production. ASOs are unable to cross the blood-brain barrier on their own, so they are administered centrally, typically achieved by intrathecal administration. Despite the clinical use of CSF-administered ASOs, there is a paucity of knowledge concerning CSF-to-brain transport mechanisms and the resulting CNS biodistribution. Here, we investigated ASO transport and distribution in the CNS following intrathecal administration, focusing on the effects of different ASO chemistries and two transport mechanisms: diffusion in the extracellular spaces and convection/dispersion in perivascular spaces (PVS) surrounding the cerebral vasculature.

We have demonstrated that intrathecal administration of fluorescently-labeled ASOs in rats leads to limited diffusion at CSF-brain and CSF-spinal cord interfaces and rapid distribution within the PVS. ASOs distributed to the PVS surrounding vessels of all type and caliber. We have also demonstrated that the extent to which perivascular distribution occurs differs in a sequence- and chemical modification-specific manner, a finding not yet reported in the literature. Furthermore, we have found that ASOs with a nucleotide sequence that allowed a random coil conformation had a significantly smaller hydrodynamic size compared to ASOs that formed secondary structures and that smaller hydrodynamic size correlated with more extensive diffusion and

perivascular access. The difference in perivascular signal between the PS-ASO and the 2'MOE-ASO was significant when quantified and was particularly apparent in the dorsal cortex as well as in subcortical brain regions such as the striatum and hippocampus.

Biodistribution and transport studies such as those conducted in the present work may provide an improved framework for understanding ASO delivery to brain and spinal cord targets. It is our hope that this framework may assist in developing ASO therapies for optimal CNS distribution to improve treatment results for devastating neurological conditions.

TABLE OF CONTENTS

PROLOGUE
Brynna Wilken-Resman

Antisense oligonucleotide (ASO) therapeutics, broadly classified as single-stranded DNA or RNA, hold promise as effective disease-modifying treatments for a large variety of disorders in which a genetic abnormality is known. Chemical modifications to the single-stranded ASOs have improved the pharmacokinetics and efficacy of these polyanionic macromolecules, with encouraging results for patients with peripheral and central nervous system (CNS) disorders. [1] However, there is yet incomplete knowledge of the distribution and transport mechanisms relevant for understanding and optimizing ASO treatment of CNS disorders. Since ASOs used in the clinic to treat CNS disorders are administered directly into the CSF via an intrathecal lumbar injection,[2,3] the understanding of ASO distribution to target brain and spinal cord regions is tied to an improving, yet incomplete understanding of movement of CSF and transport of CSF-borne solutes to brain and spinal cord tissue. [4] This dissertation is intended to enhance the understanding of CNS distribution of ASOs and examine the factors important for effective distribution of macromolecule therapeutics administered into the CSF.

Chapter one provides a review of important developments in understanding CSF movement and flow through CSF spaces, particularly the anatomy and physiology of perivascular spaces (PVS) from initial observations to its suggested function as a delivery conduit for therapeutics administered into the CSF. This chapter also explains the origins and meanings of several terms related to fluid movement in the CNS. Interchangeable use of these terms which do not describe interchangeable anatomical features or processes has contributed to confusion within the field.

Chapter two summarizes the use and development of ASO therapeutics for CNS disorders and places the present research in this context.

Chapter three describes the CNS distribution of two different ASOs of similar molecular weight and charge following intrathecal infusion at the cisterna magna. These two ASOs differed, however, in their nucleotide sequence and chemical modifications to the backbone and sugar, providing an opportunity to understand the impact of these modifications on the resulting CNS distribution. The structures of these ASOs, the phosphorothioate ASO (PS-ASO) and 2'-O-methoxy ethyl gapmer (2'MOE), are found in Figure 1.

Chapter four similarly examines the CNS distribution of an ASO after intrathecal administration, but the chemical modifications (morpholine ring and phosphorodiamidate backbone) are such that the negative charge typical of ASOs is eliminated and protein binding is minimal. The structure of this ASO, the phosphorodiamidate morpholino oligonucleotide (PMO), is found in Figure 1.

The chapters contained in this dissertation strive to align the fields of research involving CNS physiology and transport mechanisms with those involving antisense oligonucleotide therapy. This is achieved through examining the distribution after intrathecal administration of ASOs with varying size, protein binding capability, and charge. The findings from the present work have relevance for clarifying the role of these properties in CNS transport mechanisms and for the development of ASO therapeutics to optimize delivery to target sites in the brain and spinal cord.

1. Bennett CF. Therapeutic Antisense Oligonucleotides Are Coming of Age. *Annu Rev Med*. 2019;70(1):307-321. doi:10.1146/annurev-med-041217-010829

2. Khorkova O, Wahlestedt C. Oligonucleotide therapies for disorders of the nervous system. *Nat Biotechnol*. 2017;35(3):249-263. doi:10.1038/nbt.3784

3. Rinaldi C, Wood MJA. Antisense oligonucleotides: The next frontier for treatment of neurological disorders. *Nat Rev Neurol*. 2018;14(1):9-22. doi:10.1038/nrneurol.2017.148

4. Abbott NJ, Pizzo ME, Preston JE, Janigro D, Thorne RG. The role of brain barriers in fluid movement in the CNS: is there a ‘glymphatic’ system? *Acta Neuropathol*. 2018;135(3):387-407. doi:10.1007/s00401-018-1812-4

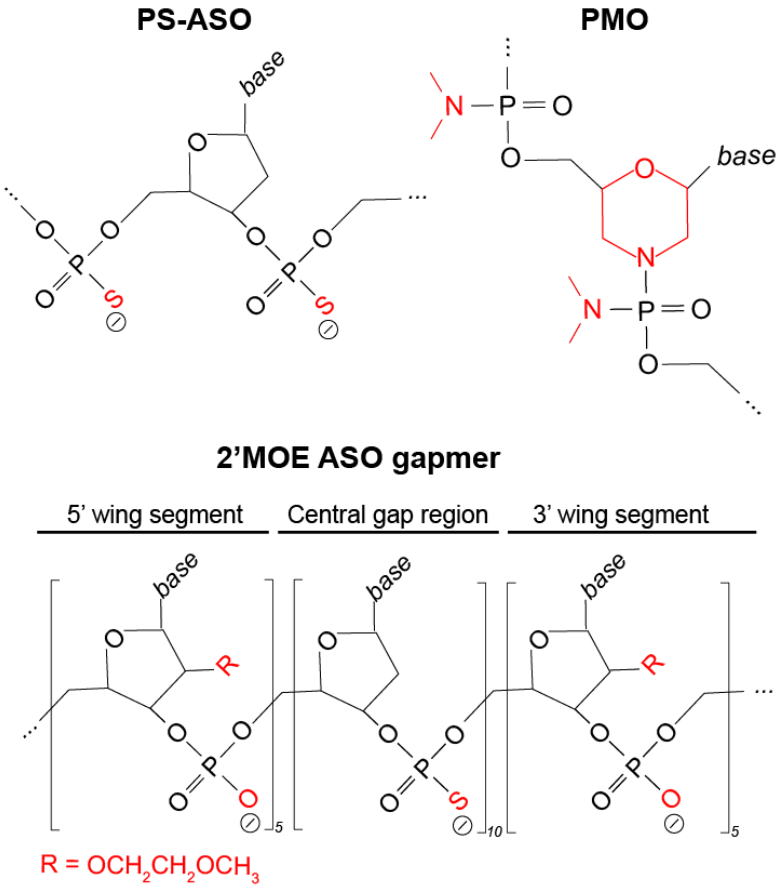

Figure 1: Structures of the ASO chemical modifications examined in Chapters 3 and 4. **PS-ASO:** One non-bridging oxygen on each phosphodiester linkage is exchanged for sulfur. **2'MOE-ASO gapmer:** The 2'-O-methoxy ethyl modification is located on the 5' and 3' wing segments. Linkages are phosphorothioate in the central 'gap' region but are traditional phosphodiester in the wing segments. **PMO**: A phosphorodiamidate backbone is substituted for the natural DNA phosphodiester backbone. A morpholine ring is substituted in place of the typical ribose or deoxyribose ring. **Fluorophore:** AlexaFluor488 was covalently attached on the 5' end of both the PS-ASO and the 2'MOE-ASO. Carboxyfluorescein was covalently attached on the 5' end of the PMO.

CHAPTER 1

The perivascular space: History and terminology

Brynna Wilken-Resman[1] and Robert Thorne[1,2]
[1]School of Pharmacy, Division of Pharmaceutical Sciences; University of Wisconsin-Madison, Madison, Wisconsin, USA [2]Denali Therapeutics, San Francisco, California, USA

Introduction

The perivascular space (PVS) is a term which, in the present work, refers to the vessel wall surrounding the endothelial cells that provide the boundary to the blood vessel lumen. This includes the vascular connective tissue space (analogous to the tunica adventitia) and potentially the basement membrane of the smooth muscle layer (analogous to the tunica media). According to this definition, the PVS within the brain and spinal cord is bounded on the blood vessel side by the endothelium (tunica intima) and on the parenchymal side by astrocyte endfeet. Our current understanding of the role of the PVS in solute transport is that it is a fluid- and connective tissue- filled compartment that allows rapid movement of solutes via convection or dispersion. It is additionally thought that this movement may form a circulation involving inflow associated with the PVS of arteries and arterioles down to the level of the capillary, diffusion (or potentially convection) to the post-capillary venule, and outflow surrounding venules and veins, although the field has yet to come to a consensus regarding directionality of flow. A visual depiction of our current conception of the PVS and its location with respect to the subarachnoid space, subpial space, and brain parenchyma is found in Figure 1 (adapted from Pizzo et al, 2018).[1]

The purpose of this discussion is to acknowledge the historical work that has contributed to the current understanding of the PVS and to provide clarification for several terms that have been used interchangeably with ‘perivascular space’ or that describe the compartments surrounding CNS vasculature in another way.

Early descriptions of a compartment surrounding vessels in pathology and normal brain

Early reports of a compartment or space surrounding cerebral blood vessels were made in the mid-1800s, much of it translated and reviewed in the following decades. In 1849 Pestalozzi noted hemorrhage into blood vessel walls in the brain–roughly describing what is now considered the perivascular space. [1] Two years later, Virchow described a sub-adventitial space and, importantly, suggested that this space extends to the capillaries and venules. [2] Robin's work in 1859 disagreed with Virchow's, reporting the space as located within the adventitia itself. [2] Whereas Pestalozzi and Virchow had described a vessel wall compartment present in pathological situations, Robin found that this compartment was present in normal brain. [1] The PVS is now sometimes called the 'Virchow-Robin' space despite Virchow and Robin's disagreement regarding the anatomy of this compartment. It should be noted that publications from the mid- to late- 1800s show that the terms 'perivascular', 'perivascular canals' and 'perivascular spaces' have been in use since some of the earliest descriptions of a compartment between the vessel endothelium and the tissue of the brain and spinal cord. [3,4]

Early work suggesting a lymphatic function of the PVS

A potential lymphatic function of the PVS was first proposed by His in the 1860s. He described the perivascular space within the brain as being in communication with the subpial space (but not the subarachnoid space). This work was among the first to involve injection of tracers into the brain parenchyma and the PVS, by which His showed perivascular spaces around all cerebral blood vessels, with the PVS width narrowing as the vessels narrowed. He reported that the PVS could act as a fluid and waste outflow path, stating, "*I think I am able to maintain for the brain then that the perivascular spaces are lymph spaces*" which he believed connected to "*lymphatic*

tubes of the pia mater" and some unknown mechanism for extracranial drainage. [3] His' lymphatic observations were controversial, and some researchers later suggested they were artifacts[1], but Tuke in 1894 revived the idea, stating, "*The body of the cell is encapsulated by a projection of the hyaline sheath of its nutrient capillary (p.v.s), the perivascular space so formed being the commencement of the lymph-path which leads from the cell to the main lymphatics of the head and neck. The brain has no true lymphatics and is instead dependent on the perivascular system for the removal of effete and superfluous material*." [5]

Key and Retzius in 1876 reviewed much of the preceding literature and were among those who disputed the lymphatic space described by His. They also produced work suggesting that the PVS surrounding blood vessels in the brain contained projections of the leptomeninges [5,6] although at this time, there was confusion regarding the anatomy of the meninges.

Many experiments involving tracer injection into the subarachnoid space up to the early 1900s had been done at rates or volumes which caused elevated pressures. Weed, in a series of experiments beginning in 1914, used hypertonic saline infused intravenously in conjunction with tracers injected into the subarachnoid space because he believed the osmotic difference would be necessary to 'pull' the tracer into the perivascular space in the absence of elevated pressure. Based on these experiments Weed described tracer distribution along the entire vascular tree, including surrounding arteries, veins, and capillaries. It should be noted that although Weed thought the PVS was in communication with the subarachnoid space, he considered the PVS to be restricted to the vessels in the parenchyma and not around vessels in the subarachnoid space.[7,8]

Patek (1944) considered much of the anatomical spaces described by His to be artifact, specifically the portion by which His thought the PVS might communicate with the perineuronal

space and also believed the space described by His (between the outer portion of the perivascular sheath and the glia) was artifact. [1,9] Patek did, however, suggest that the 'true' perivascular space communicates with the brain tissue and that the perivascular space at the level of the capillary had no outer anatomical barrier. He therefore described the perivascular space at the capillaries as a location where CSF-ISF (interstitial fluid) mixing could occur, stating "*The walls of these* [perivascular] *spaces terminate at the beginning of the capillaries and their fluid contents become continuous with the tissue fluid of the brain. It may be concluded, therefore, that no anatomical barrier exists between brain capillary wall and neural tissue and that through the perivascular spaces the neural tissue fluid is directly continuous with cerebrospinal fluid*." [1]

Improvements in techniques and microscopy yield more detailed understanding of the PVS and connections with the subarachnoid space and subpial space

The continuity of the PVS surrounding cranial (and some extracranial) vessels was proposed by Foldi, who called the PVS 'prelymphatics'. [10,11] Further work by Szentistvanyi and colleagues confirmed that the PVS of parenchymal vessels was continuous with the PVS of subarachnoid space leptomeningeal vessels but disputed the extension to extracranial vessels proposed by Foldi. [8]

Electron microscopy work by Zervas showed that leptomeningeal vessels in the subarachnoid space of cats appeared to contain pores or 'stomata' with dense tangles of fibrous connective tissue visible underneath the pore in the vessel adventitia. [12] These pores were confirmed on the rat leptomeningeal vessels by electron microscopy years later by Pizzo, Kumar, and Thorne, who hypothesized that they might act as a size-dependent access point to the perivascular space from the subarachnoid space. [13] Access to the PVS from the subarachnoid space may also be possible

through gaps between adventitial cells lining leptomeningeal vessels, as demonstrated by electron microscopy performed by Fredrickson and Low[14] and again by Cloyd and Low. [15] Connections between the subpial space and PVS were demonstrated by electron microscopy by Krisch and colleagues[16] and by Hutchings and Weller, who also noted that the cells lining leptomeningeal vessels in the subarachnoid space were pial in origin. [17]

Bulk flow or dispersion within the PVS

Evidence for bulk flow via the perivascular space was discussed by Cserr and colleagues after their 1977 work showed that tracers injected into the parenchyma showed size-independent clearance compatible with bulk flow. This work also suggested that ISF exited the brain via the perivascular spaces, mixing with the CSF. [18] Further evidence for bulk flow in the perivascular space was compiled by Ichimura[19] as well as Rennels[20] and Abbott[21], among others.

The dimensions of the PVS are relevant in that they must be wide enough if convection is to occur. Using electron microscopy, Ichimura and colleagues reported a width of up to 10 μm for the perivascular space of the leptomeningeal vessels in rats, noting that the width decreased around smaller vessels. [19] In the same publication, they reported that the perivascular space of vessels in the subarachnoid space was continuous with the perivascular space in the cortex as well as with the subpial space. They stated that the PVS consisted of the adventitia of the vessel wall (and not the smooth muscle of the tunica media).[19] The idea that the PVS consisted of the vessel adventitia, or connective tissue space, had been suggested since Robin in the 1800s and reiterated many times since. However, perivascular distribution may also occur in the media, or smooth muscle basement membrane between the adventitial and endothelial layers. CSF- or

intraparenchymal- injected tracer distribution to the smooth muscle basement membrane has been demonstrated in a number of more recent studies. [13,22,23]

Directional bulk flow within the PVS and arterial pulsations as a driving force

The 1985 work by Rennels involving ventricular infusion of horseradish peroxidase showed a 'paravascular' circulation characterized by inflow surrounding arterioles and outflow surrounding venules, with the basement membranes of capillaries providing the connection from inflow to outflow. Rennels used the term 'paravascular' because he believed 'perivascular space' to be a term for the compartment surrounding arterioles and venules but not continuing to the level of the capillary and he wanted a term that would refer to a compartment compatible with directional flow surrounding arterioles, capillaries, and venues. [20] Although Cserr and colleagues did not find evidence of a 'circulation', as they did not detect directionality to bulk flow within the PVS[19], Weller's work involving tracer injection into the subarachnoid space supported the idea of directionality of bulk flow and confirmed that tracer could be found in the PVS of arteries and veins and surrounding capillaries. [24]

Advancements in imaging capability including *in vivo* two-photon imaging yielded evidence to support the idea that there may be a circulation (inflow within the PVS of arterioles and outflow within the PVS of venules). [25] This work, by Iliff and Nedergaard, also demonstrated tracer distribution around microvessels. Unlike Rennels, Iliff and Nedergaard did not interpret these results to suggest the basement membranes or a space surrounding capillaries as a connection between the PVS of arterioles and venules and instead suggested bulk flow through the extracellular spaces from the PVS of arterioles to the PVS of venules aided by aquaporin-4 water channels found on astrocytes (glial cells). Iliff and Nedergaard termed this interpretation the

'glymphatic' system based on the proposed role of glia and the long-held idea that the PVS could have a lymphatic function. Although the imaging results demonstrating directional bulk flow within the PVS of arterioles and venules and tracer distribution to the microvessel level are in general agreement with other experimental work in the field, certain aspects of the 'glymphatic' system have been scrutinized, particularly the involvement of glia[26] and the suggestion of bulk flow through the narrow extracellular spaces. [27]

Rennels also performed experiments with reduced and eliminated arterial pulsation. The results demonstrating reduced perivascular transport suggested that bulk flow in the PVS might be driven by arterial pulsations. [20] Mathematical modeling later performed by Linninger and colleagues further detailed the role of vascular expansion and constriction on CSF flow. [28] Although most experimental evidence and some modeling-based evidence has suggested bulk flow driven by arterial pulsation as the transport process by which fluid flows through the PVS, it is worth noting that other mathematical models have predicted dispersion as the transport mechanism as opposed to bulk flow or convection and disputed the ability of arterial pulsation to drive fluid flow. [29] Dispersion would also result in fast fluid transport but differs from convection in that it involves a combination of fluid mixing and diffusion that is non-directional.

Peri-capillary CSF and CSF-borne solute transport

The question of whether there is peri-capillary transport of CSF-administered solute is important for understanding the relevance of the PVS as a conduit for drug delivery since neurons are typically within 10-20 μm from the nearest capillary. [30,31] A recent publication examining the basement membranes associated with the perivascular space provided an in-depth molecular characterization of the PVS. [32] This publication demonstrated interconnected perivascular spaces

from arterioles to venules, including a potential perivascular space surrounding capillaries, as they showed that the parenchymal and endothelial basement membranes were not fused. Despite this evidence suggesting a potential fluid space surrounding capillaries, there is not consensus, with several groups having suggested that CSF movement occurs along capillary basement membranes[14,33] or connective tissue. [34]

Olfactory drainage pathway

Early work examining the perivascular space was in large part carried out to learn more about lymphatic function in the CNS and CSF or waste drainage pathways and by the late 1800s and early 1900s, substantial evidence suggested that a drainage route existed along an olfactory pathway. Faber, who, reviewed much of this work in 1937 and contributed his own findings[35], noted that Schwalbe, in 1869, was the first to report that substances injected into the subarachnoid space appeared in the lymphatics of the nasal mucosa. Key and Retzius then performed similar experiments, showing that dye injected into the subarachnoid space crossed the cribriform plate and was located in the nasal mucosa as well as along olfactory nerves[35] and drained to the cervical lymph nodes.[36] Weed also examined the nasal passages in his experiments using intravenous hypertonic saline with subarachnoid tracer injection and showed that drainage occurred along the olfactory nerves to the connective tissue in the nasal mucosa and was then absorbed into the nasal lymphatics[35] and drained to the cervical lymph nodes[36], although he appeared to believe that under normal circumstances an olfactory drainage pathway was secondary to drainage via arachnoid villi to the dural venous sinuses. [7] Mortensen and Sullivan further studied the olfactory drainage pathway via subarachnoid injections of gelatin, stating, "*On dissection it became clear that the deeper* [deep cervical lymph] *nodes were filling by way*

of the nasal cavity…[the gelatin] *passes from the subarachnoid space along the olfactory nerves to the nasal mucosa and then by way of lymph vessels along the pharynx to the upper deep cervical nodes*." [36] Faber's 1937 work agreed with this conception of an olfactory drainage pathway, and this work added two pieces of information: that a radiocontrast agent injected into the nasal mucosa could reach the brain via these same connections and that radiocontrast-filled perivascular spaces crossed the cribriform plate and could be another route for drainage along the olfactory pathway. [35] Further evidence for CSF drainage to cervical lymphatics via an olfactory route was collected using a variety of tracers by Szentistvanyi[8], Kida and Weller[37], Pizzo[13], Wilken-Resman (unpublished, Chapters 3 & 4), and many others.

Although much work focused on drainage via an olfactory pathway, there was also work showing drainage to the venous sinuses via the arachnoid villi, which became the classical understanding of CSF clearance, as well as early work demonstrating lymphatics in the dura. [38,39] This concept was revisited in greater detail in two publications in 2015[40,41] although more work will be necessary to determine the precise connections for drainage via dural lymphatics.

Evidence from tracer studies suggest that the drainage of ISF and CSF may be compartmentalized. Tracers injected intraparenchymally have been found to drain preferentially to ipsilateral cervical lymph nodes[8,42] whereas tracers injected into the CSF drain to the cervical lymph nodes on both sides. [8,13,37] Further research will be required to determine the exact drainage pathways of CSF and ISF.

IPAD and pial-glial transport: Recent alternative conception of CSF passage surrounding arteries

Through tracer experiments, Carare and colleagues recently developed an idea that fluid flow into the brain occurs within the "pial-glial basement membrane" surrounding the smooth muscle layer of the arterial wall (they believe the pia and glia limitans are fused) and that fluid outflow occurs within the smooth muscle basement membrane surrounding arteries/arterioles. This outflow pathway they call 'intramural periarterial drainage' (IPAD). Veins/venules do not play any role according to this pial-glial inflow and IPAD outflow conception. [43]

PVS as a delivery conduit for CSF-administered therapeutics

The intention behind much of the historical work regarding the anatomy and physiology of the perivascular space was to better understand CSF and ISF movement and to examine drainage of these fluids to extracranial sites. However, with the approval of three CSF-administered therapeutics within the last decade (a small peptide, an antisense oligonucleotide, and a protein) a line of research has extended to better understand the potential for macromolecule therapeutic delivery via CSF transport mechanisms including diffusion from the CSF-facing pial surface and, importantly, rapid convection or dispersion via the PVS. Important features that may potentially facilitate efficient therapeutic distribution in the CNS including size-dependent access to the tunica media and low-resistance pericapillary transport were detailed by Pizzo and colleagues[13] and research regarding the impact of size, charge, and binding of macromolecule therapeutics has been conducted (Wilken-Resman and Thorne, unpublished, Chapters 3 & 4).

Use of the term 'perivascular space'

One reason we prefer the term 'perivascular space' or 'PVS' is because it's generic enough to grow with new developments and understanding—perivascular space refers to a compartment surrounding (*peri*-) the vasculature. As laid out in this chapter, the understanding of the anatomy and physiology of the PVS has changed a great deal and it is useful to have an adaptable term. Terminology such as 'Virchow-Robin space' is somewhat confusing since it is specific to the conception of two researchers who did not agree on the anatomy of that space, and terminology including 'intramural periarterial drainage', 'pial-glial basement membrane' 'glymphatic', and even 'paravascular' are tied to other ideas such as direction of flow, involvement of specific cell types, and/or physiological functions which are not necessarily widely accepted. A second reason why we use the term 'perivascular space' is based on the ubiquitous use of this term throughout the many years of research regarding the anatomy, physiology, and function of the fluid- and connective tissue- filled spaces surrounding the cerebrovasculature. It is expected that enhancements in techniques and imaging will continue to result in a more detailed understanding of the anatomy and physiology of the perivascular space in the future. Use of this term provides continuity throughout the literature and the ability to trace the major developments in the field.

1. Patek PR. The perivascular spaces of the mammalian brain. *Anat Rec*. 1942;88(1):1-24. doi:10.1086/265545

2. Deecke T. On the perivascular spaces in the nervous system. *J Insa*. 1874:322-330.

3. His W, Bastian HC. On a System of Perivascular Canals in the Nerve Centres, and on their Relationship to the Lymphatic System. *J Anat Physiol*. 1867;1(2):347-352.

4. Tuke JB. On the Morbid Histology of the Brain and Spinal Cord as Observed in the Insane. *Br foreign medico-chirurgical Rev*. 1873:450-460.

5. Tuke JB. *The Insanity of Over-Exertion of the Brain: Being the Morison Lectures Delivered before the Royal College of Physicians of Edinburgh*.; 1894.

6. Millen JW, Woollam DH. The reticular perivascular tissue of the centra nervous system. *J Neurol Neurosurg Psychiatry*. 1954;17(4):286-294. doi:10.1136/jnnp.17.4.286

7. Weed LH. The absorption of cerebrospinal fluid into the venous system. *Am J Anat*. 1923;31(3):191-221. doi:10.1002/aja.1000310302

8. Szentistvanyi I, Patlak CS, Ellis RA, Cserr HF. Drainage of interstitial fluids from different regions of the rat brain. *Ren Physiol*. 1984;246(6):835-844.

9. Woollam DH, Millen JW. The perivascular spaces of the mammalian central nervous system and their relation to the perineuronal and subarachnoid spaces. *J Anat*. 1955;89(2):193-200. http://www.ncbi.nlm.nih.gov/pubmed/14367214%0Ahttp://www.pubmedcentral.nih.gov/articlerender.fcgi?artid=PMC1244781.

10. Casley Smith JR, Foldi Borcsok E, Foldi M. The prelymphatic pathways of the brain as revealed by cervical lymphatic obstruction and the passage of particles. *Br J Exp Pathol*. 1976;57(2):179-188.

11. Casley Smith JR, Clodius L, Foldi Borcsok E, Gruntzig J, Foldi M. The effects of chronic lymphostasis on regions drained by lymphatics and prelymphatics. *J Pathol*. 1978;124(June 1977).

12. Zervas NT, Liszczak TM, Mayberg MR, Black PM. Cerebrospinal fluid may nourish cerebral vessels through pathways in the adventitia that may be analogous to systemic vasa vasorum. *J Neurosurg*. 1982;56(4):475-481. doi:10.3171/jns.1982.56.4.0475

13. Pizzo ME, Wolak DJ, Kumar NN, et al. Intrathecal antibody distribution in the rat brain: surface diffusion, perivascular transport and osmotic enhancement of delivery. *J Physiol*. 2018;596(3):445-475. doi:10.1113/JP275105

14. Frederickson RG, Low FN. Blood vessels and tissue space associated with the brain of the rat. *Am J Anat*. 1969;125(2):123-145. doi:10.1002/aja.1001250202

15. Cloyd MW, Low FN. Scanning Electron Microscopy of the Subarachnoid Space in the Dog. *J Comp Neurol*. 1974;153:325-368.

16. Krisch B, Leonhardt H, Oksche A, Institut A, Kiel DU. Compartments and perivascular arrangement of the meninges covering the cerebral cortex of the rat. *Celll Tissue Res*.

1984;238:459-474.

17. Hutchings M, Weller RO. Anatomical relationships of the pia mater to cerebral blood vessels in man. *J Neurosurg*. 1986;65:316-325.

18. Cserr H, Cooper DN, Milhorat TH. Flow of Cerebral Interstitial Fluid as Indicated by the Removal of Extracellular Markers from Rat Caudate Nucleus. *Exp Eye Res*. 1977;25:461-473.

19. Ichimura T, Fraser PA, Cserr HF. Distribution of extracellular tracers in perivascular spaces of the rat brain. *Brain Res*. 1991;545(1-2):103-113. doi:10.1016/0006-8993(91)91275-6

20. Rennels ML, Gregory TF, Blaumanis OR, Fujimoto K, Grady PA. Evidence for a "Paravascular" fluid circulation in the mammalian central nervous system, provided by the rapid distribution of tracer protein throughout the brain from the subarachnoid space. *Brain Res*. 1985;326(1):47-63. doi:10.1016/0006-8993(85)91383-6

21. Abbott NJ. Evidence for bulk flow of brain interstitial fluid: Significance for physiology and pathology. *Neurochem Int*. 2004;45(4):545-552. doi:10.1016/j.neuint.2003.11.006

22. Carare RO, Bernardes-Silva M, Newman TA, et al. Solutes , but not cells , drain from the brain parenchyma along basement membranes of capillaries and arteries : significance for cerebral amyloid angiopathy and neuroimmunology. *Neuropathol Appl Neurobiol*. 2008;34:131-144. doi:10.1111/j.1365-2990.2007.00926.x

23. Weller RO, Subash M, Preston SD, Mazanti I, Carare RO. Perivascular Drainage of Amyloid- b Peptides from the Brain and Its Failure in Cerebral Amyloid Angiopathy and Alzheimer's Disease. *Brain Pathol*. 2008;18(92):253-266. doi:10.1111/j.1750-3639.2008.00133.x

24. Zhang ET, Richards HK, Kida S, Weller RO. Directional and compartmentalised drainage of interstitial fluid and cerebrospinal fluid from the rat brain. *Acta Neuropathol*. 1992:233-239.

25. Iliff JJ, Wang M, Liao Y, et al. A paravascular pathway facilitates CSF flow through the brain parenchyma and the clearance of interstitial solutes, including amyloid β. *Sci Transl Med*. 2012;4(147):147ra111-147ra111. doi:10.1126/scitranslmed.3003748

26. Smith AJ, Yao X, Dix JA, Jin BJ, Verkman AS. Test of the 'glymphatic' hypothesis demonstrates diffusive and aquaporin-4-independent solute transport in rodent brain parenchyma. *Elife*. 2017;6:1-16. doi:10.7554/eLife.27679

27. Abbott NJ, Pizzo ME, Preston JE, Janigro D, Thorne RG. The role of brain barriers in fluid movement in the CNS: is there a 'glymphatic' system? *Acta Neuropathol*. 2018;135(3):387-407. doi:10.1007/s00401-018-1812-4

28. Tangen K, Mehta AI, Linninger AA. Cerebrospinal Fluid Dynamics and Intrathecal Delivery. In: Krames E, Peckham PH, Rezai A, eds. *Neuromodulation*. 2nd ed. Elsevier Ltd; 2018:829-846. doi:10.1016/B978-0-12-805353-9.00067-X

29. Asgari M, Zélicourt D De, Kurtcuoglu V. Glymphatic solute transport does not require

bulk flow. *Sci Rep*. 2016;6(38635):1-11. doi:10.1038/srep38635

30. Lovick TA, Brown LA, Key BJ. Neurovascular relationships in hippocampal slices: Physiological and anatomical studies of mechanisms underlying flow-metabolism coupling in intraparenchymal microvessels. *Neuroscience*. 1999;92(1):47-60. doi:10.1016/S0306-4522(98)00737-4

31. Mabuchi T, Lucero J, Feng A, Koziol JA, Del Zoppo GJ. Focal cerebral ischemia preferentially affects neurons distant from their neighboring microvessels. *J Cereb Blood Flow Metab*. 2005;25(2):257-266. doi:10.1038/sj.jcbfm.9600027

32. Hannocks MJ, Pizzo ME, Huppert J, et al. Molecular characterization of perivascular drainage pathways in the murine brain. *J Cereb Blood Flow Metab*. 2018;38(4):669-686. doi:10.1177/0271678X17749689

33. Maynard EA, Schultz RL, Pease DC. Electron microscopy of the vascular bed of rat cerebral cortex. *Am J Anat*. 1957;100(3):409-433.

34. Cervós-Navarro J, Ferszt R. Connective tissue in pericapillary spaces of the human spinal cord. *Acta Neuropathol*. 1973;24(2):178-183. doi:10.1007/BF00684839

35. Faber WM. The nasal mucosa and the subarachnoid space. *Am J Anat*. 1937;62(1):121-148. doi:10.1002/aja.1000620106

36. Mortensen OA, Sullivan WE. The cerebrospinal fluid and the cervical lymph nodes. *Anat Rec*. 1933:359-363.

37. Kida S, Pantazis A, Weller RO. CSF drains directly from the subarachnoid space into nasal lymphatics in the rat. Anatomy, histology and immunological significance. *Neuropathol Appl Neurobiol*. 1993;19(6):480-488. doi:10.1111/j.1365-2990.1993.tb00476.x

38. Jacobi W. Das Saftspaltensystem der Dura. *Arch Psychiatr Nervenkr*. 1924;70(1):269-285. doi:10.1007/BF01814082

39. Földi M, Gellért A, Kozma M, Poberai M, Zoltán OT, Csanda E. New contributions to the anatomical connections of the brain and the lymphatic system. *Acta Anat (Basel)*. 1966;64(4):498-505. doi:10.1159/000142849

40. Aspelund A, Antila S, Proulx ST, et al. A dural lymphatic vascular system that drains brain interstitial fluid and macromolecules. *J Exp Med*. 2015;212(7):991-999. doi:10.1084/jem.20142290

41. Louveau A, Smirnov I, Keyes TJ, et al. Structural and functional features of central nervous system lymphatic vessels. *Nature*. 2015;523(7560):337-341. doi:10.1038/nature14432

42. Bradbury MW, Cserr HF, Westrop RJ. Drainage of cerebral interstitial fluid into deep cervical lymph of the rabbit. *Am J Physiol Physiol*. 1981;240:F329-F336.

43. Albargothy NJ, Johnston DA, Macgregor M, et al. Convective influx / glymphatic system : tracers injected into the CSF enter and leave the brain along separate periarterial

basement membrane pathways. 2018:139-152.

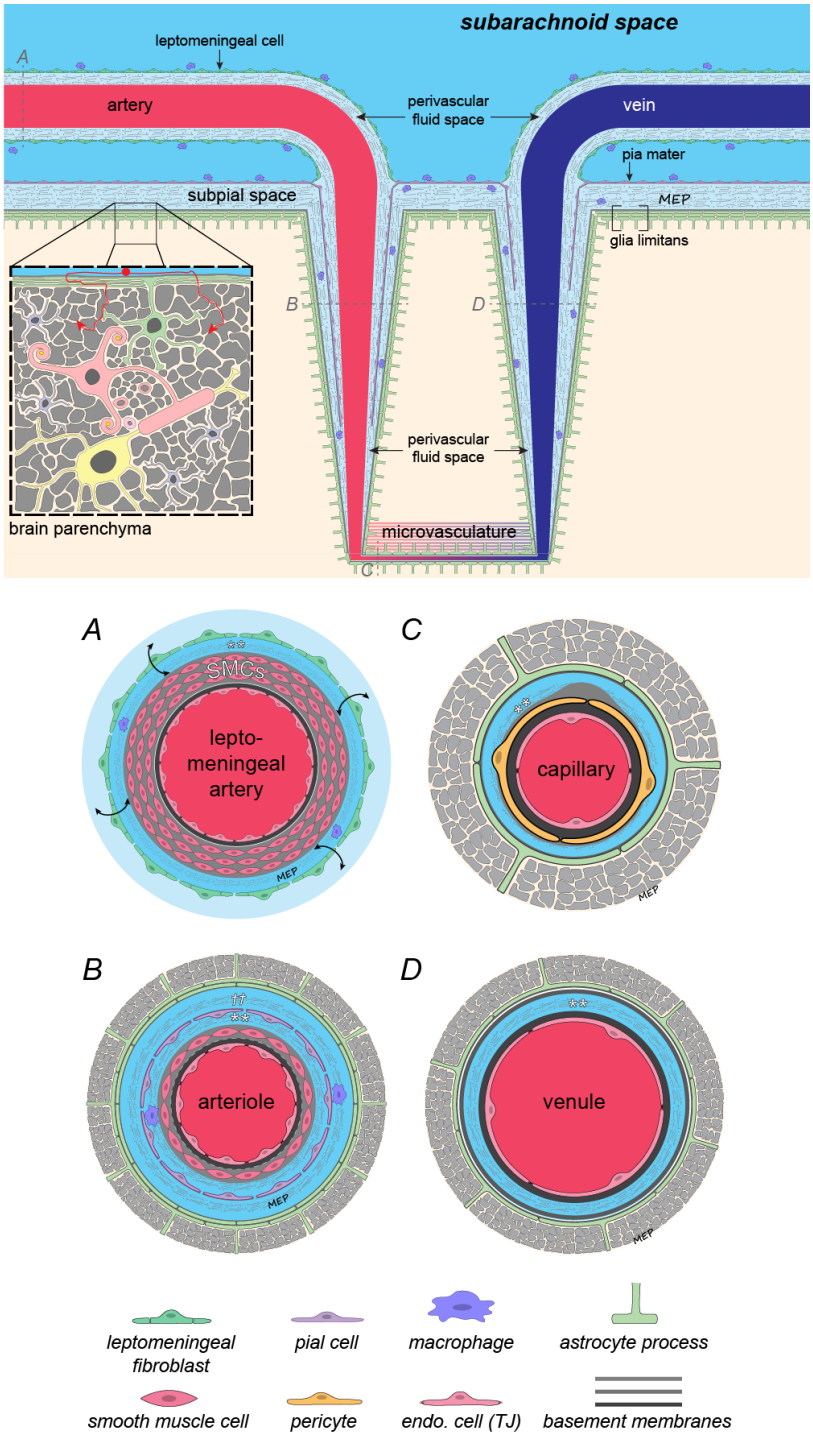

Figure 1: Schematic of the perivascular space, subarachnoid space, and subpial space. A-D show vessel cross-sections. The vessel adventitia is indicated by (**), while (††) denotes continuation

with the subpial space. ‘SMC’ indicates smooth muscle cells. Figure adapted from Pizzo, *J Physiol*, 2018.

CHAPTER 2
Antisense oligonucleotide therapeutics for disorders of the central nervous system

Brynna Wilken-Resman[1] and Robert Thorne[1,2]
[1]School of Pharmacy, Division of Pharmaceutical Sciences; University of Wisconsin-Madison, Madison, Wisconsin, USA [2]Denali Therapeutics, San Francisco, California, USA

Antisense oligonucleotide therapeutics for central nervous system disorders

The potential for antisense oligonucleotides (ASOs) to be used as therapeutics has been known for nearly 50 years, yet it was not until 2016, with the approval of two ASOs—eteplirsen[1] and nusinersen[2]—that the promise of ASOs as effective therapeutics began to come to fruition. [3,4] ASOs are attractive as a drug class because they are disease-modifying therapeutics–they act at the root of the problem by targeting the genetic code at the level of pre-mRNA or mRNA as opposed to ameliorating symptoms. [3] ASO therapies have made progress in engaging targets that are often considered difficult to treat by more traditional small molecule therapeutics.[5] This was demonstrated by the approval of both eteplirsen for Duchenne muscular dystrophy and nusinersen for spinal muscular atrophy, both often fatal disorders manifesting in children with no previous treatments to significantly impact prognosis.[1,2] The approval of nusinersen was particularly impactful because it is the first ASO (and second macromolecule therapeutic overall) that is administered into the cerebrospinal fluid and engages its targets in the central nervous system (CNS).

For the current purposes, the term ‘antisense oligonucleotides’ or ‘ASO’ will be used to reference single stranded DNA or chimeric DNA/RNA that hybridize to their complementary RNA but does not refer to double stranded RNA (siRNA, RNAi) or aptamers, which are single stranded oligonucleotides that fold into a 3D structure and bind to proteins. [6]

Chemical modifications of ASOs and their effects on ASO properties

Backbone chemistry is important for the pharmacokinetics of ASOs. Natural phosphodiester internucleoside linkages are vulnerable to degradation by exonucleases[7,8] and rapid renal

excretion.[8] The most common backbone modification is the substitution of a sulfur for a non-bridging oxygen to form a phosphorothioate internucleoside linkage. The development of the phosphorothioate backbone was a major advance. The phosphorothioate modification protects against degradation by nucleases but is not completely resistant. [8] Incorporation of a phosphorothioate backbone has a dramatic effect on pharmacokinetics as it increases binding to plasma proteins, thereby reducing renal excretion, increasing the half-life, and shifting distribution away from the kidneys and towards other tissues. [8–10] A major binding partner for phosphorothioate ASOs is albumin, which has been shown to bind in the micromolar range.[9,11] Despite the benefits of protein binding for pharmacokinetics, one disadvantage to the phosphorothioate ASO's abundant protein binding is the occurrence of off-target effects and toxicity.[12] Despite this drawback, the phosphorothioate linkage is incorporated into all CSF-administered ASOs that are currently approved or in clinical trials.

Introduction of *n* phosphorothioate internucleoside linkages creates 2^n stereoisomers. [13] Wave Life Sciences has developed stereopure phosphorothioate ASOs and has published results to suggest that controlling the chirality of phosphorothioate linkages may result in improved stability and RNA degradation via RNaseH cleavage as well as a more durable response compared to stereoisomeric mixtures. [13] Two stereopure phosphorothioate ASOs are currently in Phase 1/2 clinical trials for Huntington's disease. It is noteworthy that these ASOs target only mutant huntingtin mRNA instead of all huntingtin mRNA and that the two ASOs in clinical trials target separate single nucleotide polymorphisms (SNPs). [14]

Another consequential backbone modification is the phosphorodiamidate internucleoside linkage. The phosphorodiamidate linkage is typically paired with a morpholine ring in place of

the natural ribose ring and this ASO is called the phosphorodiamidate morpholino oligonucleotide (PMO). PMOs are extremely nuclease resistant and have high affinity for their target RNA. [15] PMOs are uncharged due to the neutral phosphorodiamidate linkage. [16] While this may allow the PMO to be readily eliminated via the kidney after systemic administration[17,18], renal excretion is not a concern for intrathecally-administered PMOs. Given PMOs' neutral charge and low plasma protein binding[19], intrathecally administered PMOs may result in an intriguing CNS tissue distribution profile. Results of one study suggest that PMOs may have some advantage in 'productive' cell uptake despite having lower CNS tissue accumulation after intrathecal administration compared to a phosphorothioate- and 2'MOE- modified ASO. [20] To date, there is one PMO, eteplirsen, that is approved by the FDA. Eteplirsen is indicated for Duchenne muscular dystrophy (DMD). [21] Although DMD is sometimes classified as a neuromuscular disorder, it is excluded from Table 1 because it is administered intravenously to promote dystrophin production in muscle. [1,4,22] There are currently no PMOs in clinical trials for CNS disorders in which CSF administration is used. However, recent preclinical work using PMOs to treat CNS disorders via CSF injections have been promising. Injection of PMOs into the lateral ventricle of a mouse model of spinal muscular atrophy effectively modified *SMN2* (Survival Motor Neuron 2) splicing and increased the lifespan of the mice. [23]

Another common modification to the natural ribose ring is the 2'-O-methoxy ethyl (2'MOE) modification. The 2'MOE sugar modification blocks degradation by nucleases[8] and increases affinity for target RNA. [24] Interestingly, the addition of the 2'MOE modification has been shown to modestly weaken the binding affinity of albumin [11] but did not appear to markedly alter plasma pharmacokinetics. [8] The 2'MOE modification is often paired with a phosphorothioate

backbone. The 2'MOE modification in combination with a partial or full phosphorothioate backbone is well-studied and found in many ASOs, including the intrathecally-administered ASOs furthest along in clinical development (RG6042 for Huntington's disease and tofersen for ALS) as well as in FDA-approved nusinersen (Table 1).

There exist other modifications aside from those previously mentioned. However, they are further behind in discovery or preclinical development for peripheral and CNS disorders and therefore will not be discussed at length. These include peptide nucleic acid (PNA), constrained ethyl (cEt), locked nucleic acid (LNA), and 2'-O-methyl (2'OMe) modifications. Further information regarding these modifications can be found in other reviews. [3,4,25]

Impacts of chemical modifications on CNS transport mechanisms and distribution

Although the impacts of ASO chemical modifications in the plasma and peripheral tissues are well-studied, it is less apparent how ASO chemical modifications impact transport mechanisms and regional distribution in the CNS. Although nuclease activity in the CSF is low, there is substantial 3'—5' exonuclease activity[26] in the brain, demonstrated by rapid degradation of a phosphodiester but not a phosphorothioate ASO of the same sequence. [7] ASOs have relatively long half lives in the CSF, in the range of months. Nusinersen, which is fully phosphorothioate- and 2'MOE- modified, has a terminal half-life in the CSF of approximately 5.5 months based on population modeling across 5 clinical trials.[27] Long half-lives prove useful since they allow infrequent dosing, reducing the burden of frequent clinic visits and occurrence of adverse events that can be associated with intrathecal lumbar puncture.[10,28,29] Nusinersen, for example, is

administered in pediatric patients at 4-month intervals after the initial phase in which loading doses are administered more frequently.[30]

Evidence for perivascular association of ASOs administered via intracerebroventricular (ICV) injection was present in the literature by the early- mid-90's[7,31] but this association was not elaborated upon and ASO distribution surrounding the vasculature remained obscure until a recent publication describing ASO perivascular localization in the arterial smooth muscle of the perivascular space (PVS)[32] after intrathecal administration. Further work has demonstrated that ASOs are not only localized in the arterial smooth muscle but are also found in the vascular connective tissue space (tunica adventitia) of the vessel wall surrounding the smooth muscle (tunica media) and that perivascular access of ASOs was found to extend throughout the vascular tree to the PVS of arterioles, microvessels and venules (Wilken-Resman and Thorne, unpublished, Chapters 3 and 4).

ASOs are relatively small in comparison to other disease-modifying therapeutics, typically 6-8 kDa with an apparent hydrodynamic size of approximately 3-5 nm (Wilken-Resman and Thorne, unpublished, Chapters 3 and 4). Other disease-modifying therapeutics such as IgG antibodies and viral vectors are approximately 10 nm[33] and 20-300 nm[34] (Wolak and Thorne, unpublished), respectively. The relatively small size of ASOs is advantageous for CNS distribution since diffusion is size-dependent[35] and access to the perivascular space from the subarachnoid CSF may also consist of a size-dependent step via entry through pores or gaps between adventitial cells in leptomeningeal vessels. [36]

There is some evidence to suggest that the charge of ASOs as well as their ability to bind proteins in the CSF and CNS may impact their distribution after intrathecal administration. A phosphorothioate ASO administered intrathecally appeared to have hindered diffusion across the pial brain surface and markedly lower perivascular distribution throughout coronal brain sections compared to a protein therapeutic (single domain antibody)[36] with a similar hydrodynamic size (Wilken-Resman and Thorne, unpublished, Chapter 3).

Recently, a fluorescence polarization assay was developed to examine binding of the 20 most abundant plasma proteins to ASOs with a combination of phosphorothioate and 2'MOE modifications. [11] Several proteins examined for plasma protein binding using this assay also have relevance for understanding ASO binding in the CSF and/or CNS tissue. In addition to the well-known occurrence of albumin binding to phosphorothioate ASOs, binding of a phosphorothioate ASO with MOE modifications on the 5' and 3' wings showed a binding association constant of 1.6 μM for IgG. This information is relevant for CNS distribution because albumin exists at low concentrations in the CSF (although this concentration can increase depending on age[37,38] and disease status[39,40]) and also exists widespread throughout CNS tissue (Pizzo and Thorne, unpublished). Recent work has shown that phosphorothioate ASO binding in the presence of CSF as well as albumin at its low CSF concentration is appreciable and results in an increase in effective hydrodynamic size (Wilken-Resman and Thorne, unpublished, Chapter 3). This size increase could reduce the ability of the ASO to diffuse through the extracellular space (ECS) or access the perivascular space from the subarachnoid CSF.

ASO binding to IgG may also impact distribution. In addition to being the second most abundant CSF protein[37], IgG has been shown to be located in the vascular connective tissue space (adventitia) of the PVS (Pizzo and Thorne, unpublished). Its size appears to exclude it from the smooth muscle (media) and from distributing into the parenchyma from the PVS. Interestingly, a fully phosphorothioated ASO appeared to distribute to the PVS adventitia but did not appear to distribute appreciably to the media (Wilken-Resman and Thorne, unpublished, Chapter 3). It is possible that the fully phosphorothioated ASO may be binding to IgG within the adventitia of the PVS which could hinder its distribution to the media and to the surrounding CNS tissue.

Although the fluorescence polarization assay used to assess ASO binding to plasma yielded a small amount of information relevant for understanding CNS distribution, this assay could be of greater use for understanding ASO binding in the ECS, perivascular space, and CSF if it were expanded to examine extracellular matrix proteins and CSF proteins.

The negative charge on many ASOs, including those with native phosphodiester backbones and those with the common phosphorothioate backbone modification, may hinder its transport in the CNS via diffusion and perivascular distribution. The extracellular spaces are narrow (approximately 40-60 nm[41]) and densely filled with extracellular matrix components, such as proteoglycans with fixed negative charge. [42] Diffusion of a negatively charged macromolecule can be hindered by electrostatic interactions. [43] Negatively charged extracellular matrix proteins in the basement membrane of smooth muscle cells could also exclude polyanionic ASOs from accessing this compartment of the PVS. However, it remains to be seen whether charge screening mediated by physiological salt concentrations (~150 mM Na)[44] in the CSF and

interstitial fluid could limit the radius of electrostatic effects[45], or Debye length, of ASOs in these environments.

Conclusions

It is clear that although there has been great success in developing ASOs as effective therapeutics and much promise for their continued use in treating genetic disorders, there is considerable work that remains to understand how to optimize ASO therapeutics. It will likely be important to take factors such as ASO size, charge, and protein binding into consideration and to further investigate how these properties can aid or hinder ASO distribution in the CNS.

1. Aartsma-Rus A, Krieg AM. FDA Approves Eteplirsen for Duchenne Muscular Dystrophy: The Next Chapter in the Eteplirsen Saga. *Nucleic Acid Ther*. 2017;27(1):1-3. doi:10.1089/nat.2016.0657

2. Aartsma-Rus A. FDA Approval of Nusinersen for Spinal Muscular Atrophy Makes 2016 the Year of Splice Modulating Oligonucleotides. *Nucleic Acid Ther*. 2017;27(2):67-69.

3. Bennett CF. Therapeutic Antisense Oligonucleotides Are Coming of Age. *Annu Rev Med*. 2019;70(1):307-321. doi:10.1146/annurev-med-041217-010829

4. Scoles DR, Minikel E V., Pulst SM. Antisense oligonucleotides: A primer. *Neurol Genet*. 2019;5(2). doi:10.1212/NXG.0000000000000323

5. Corey DR. Nusinersen, an antisense oligonucleotide drug for spinal muscular atrophy. *Nat Neurosci*. 2017;20(4):497-499. doi:10.1038/nn.4508

6. Nimjee SM, White RR, Becker RC, Sullenger BA. Aptamers as Therapeutics. *Annu Rev Pharmacol Toxicol*. 2017:61-79. doi:10.1146/annurev-pharmtox-010716-104558.Aptamers

7. Whitesell L, Geselowitz D, Chavany C, et al. Stability, clearance, and disposition of intraventricularly administered oligodeoxynucleotides: implications for therapeutic application within the central nervous system. *Proc Natl Acad Sci U S A*. 1993;90(10):4665-4669. doi:10.1073/pnas.90.10.4665

8. Geary RS, Watanabe TA, Truong L, et al. Pharmacokinetic properties of 2'-O-(2-methoxyethyl)-modified oligonucleotide analogs in rats. *J Pharmacol Exp Ther*. 2000;296(3):890-897. http://www.ncbi.nlm.nih.gov/pubmed/11181921.

9. Brown DA, Kang SH, Gryaznov SM, et al. Effect of phosphorothioate modification of oligodeoxynucleotides on specific protein binding. *J Biol Chem*. 1994;269(43):26801-26805.

10. Khorkova O, Wahlestedt C. Oligonucleotide therapies for disorders of the nervous system. *Nat Biotechnol*. 2017;35(3):249-263. doi:10.1038/nbt.3784

11. Gaus HJ, Gupta R, Chappell AE, Østergaard ME, Swayze EE, Seth PP. Characterization of the interactions of chemically-modified therapeutic nucleic acids with plasma proteins using a fluorescence polarization assay. *Nucleic Acids Res*. 2018;47(3):1110-1122. doi:10.1093/nar/gky1260

12. Shen W, De Hoyos CL, Migawa MT, et al. Chemical modification of PS-ASO therapeutics reduces cellular protein-binding and improves the therapeutic index. *Nat Biotechnol*. 2019;37(6):640-650. doi:10.1038/s41587-019-0106-2

13. Iwamoto N, Butler DCD, Svrzikapa N, et al. Control of phosphorothioate stereochemistry substantially increases the efficacy of antisense oligonucleotides. *Nat Biotechnol*. 2017;35(9):845-851. doi:10.1038/nbt.3948

14. Hersch S, Claassen D, Edmondson M, Wild E, Guerciolini R, Panzara M. Multicenter, Randomized, Double-blind, Placebo-controlled Phase 1b/2a Studies of WVE-120101 and WVE-120102 in Patients with Huntington's Disease (P2.006). *Neurology*. 2017;88(16

Supplement).

15. Summerton J, Weller D. Morpholino antisense oligomers: Design, preparation, and properties. *Antisense Nucleic Acid Drug Dev*. 1997;7(3):187-195. doi:10.1089/oli.1.1997.7.187

16. Summerton J. Morpholino antisense oligomers: The case for an RNase H-independent structural type. *Biochim Biophys Acta - Gene Struct Expr*. 1999;1489(1):141-158. doi:10.1016/S0167-4781(99)00150-5

17. Heald AE, Iversen PL, Saoud JB, et al. Safety and pharmacokinetic profiles of phosphorodiamidate morpholino oligomers with activity against ebola virus and marburg virus: Results of two single-ascending-dose studies. *Antimicrob Agents Chemother*. 2014;58(11):6639-6647. doi:10.1128/AAC.03442-14

18. Geary RS, Norris D, Yu R, Bennett CF. Pharmacokinetics, biodistribution and cell uptake of antisense oligonucleotides. *Adv Drug Deliv Rev*. 2015;87:46-51. doi:10.1016/j.addr.2015.01.008

19. Sazani P, Magee T, Charleston J, et al. In Vitro Pharmacokinetic Evaluation of Eteplirsen, SRP-4045, and SRP-4053; Three Phosphorodiamidate Morpholino Oligomers (PMO) for the Treatment of Patients with Duchenne Muscular Dystrophy (DMD) (P5.061). *Neurology*. 2015;84.

20. Rigo F, Chun SJ, Norris DA, et al. Pharmacology of a Central Nervous System Delivered 2'-O-Methoxyethyl-Modified Survival of Motor Neuron Splicing Oligonucleotide in Mice and Nonhuman Primates. *J Pharmacol Exp Ther*. 2014;350(1):46-55. doi:10.1124/jpet.113.212407

21. US FDA. FDA grants accelerated approval to first drug for Duchenne muscular dystrophy. https://www.fda.gov/news-events/press-announcements/fda-grants-accelerated-approval-first-drug-duchenne-muscular-dystrophy. Published 2016.

22. Lim KRQ, Maruyama R, Yokota T. Eteplirsen in the treatment of Duchenne muscular dystrophy. *Drug Des Devel Ther*. 2017;11:533-545. doi:10.2147/DDDT.S97635

23. Osman EY, Washington CW, Kaifer KA, et al. Optimization of morpholino antisense oligonucleotides targeting the intronic repressor element1 in spinal muscular atrophy. *Mol Ther*. 2016;24(9):1592-1601. doi:10.1038/mt.2016.145

24. Freier SM, Altmann K-H. The ups and downs of nucleic acid duplex stability: structure-stability studies on chemically-modified DNA:RNA duplexes. *Nucleic Acids Res*. 1997;25(22):4429-4443. doi:10.1093/nar/25.22.4429

25. Evers MM, Toonen LJA, van Roon-Mom WMC. Antisense oligonucleotides in therapy for neurodegenerative disorders. *Adv Drug Deliv Rev*. 2015;87:90-103. doi:10.1016/j.addr.2015.03.008

26. Krishna TH, Hemkal A, Rao KS. The Presence of 3' – 5' Exonuclease Activity in Rat Brain Neurons and Its Role in Template-Driven Extension of 3' -Mismatched Primers by DNA-Polymerase Beta in Aging Neurons. *Neurochem Res*. 2004;29(4):761-770.

27. Luu KT, Norris DA, Gunawan R, Henry S, Geary R, Wang Y. Population Pharmacokinetics of Nusinersen in the Cerebral Spinal Fluid and Plasma of Pediatric Patients With Spinal Muscular Atrophy Following Intrathecal Administrations. *J Clin Pharmacol*. 2017;57(8):1031-1041.

28. Finkel RS, Mercuri E, Darras BT, et al. Nusinersen versus Sham Control in Infantile-Onset Spinal Muscular Atrophy. *N Engl J Med*. 2017;377(18):1723-1732. doi:10.1056/NEJMoa1702752

29. Tabrizi SJ, Leavitt BR, Landwehrmeyer GB, et al. Targeting Huntingtin Expression in Patients with Huntington's Disease. *N Engl J Med*. 2019:NEJMoa1900907. doi:10.1056/NEJMoa1900907

30. US FDA. Spinraza (nusinersen)-FDA. https://www.accessdata.fda.gov/drugsatfda_docs/label/2016/209531lbl.pdf.

31. Yee F, Ericson H, Reis DJ, Wahlestedt C. Cellular uptake of intracerebroventricularly administered biotin- or digoxigenin-Labeled antisense oligodeoxynucleotides in the rat. *Cell Mol Neurobiol*. 1994;14(5):475-486. doi:10.1007/BF02088832

32. Mazur C, Swayze EE, Verma A, et al. Brain pharmacology of intrathecal antisense oligonucleotides revealed through multimodal imaging Find the latest version : Brain pharmacology of intrathecal antisense oligonucleotides revealed through multimodal imaging. 2019;4(20).

33. Wolak DJ, Pizzo ME, Thorne RG. Probing the extracellular diffusion of antibodies in brain using in vivo integrative optical imaging and ex vivo fluorescence imaging. *J Control Release*. 2015;197:78-86. doi:10.1016/j.jconrel.2014.10.034

34. Davidson BL, Breakefield XO. Viral vectors for gene delivery to the nervous system. *Nat Rev Neurosci*. 2003;4(5):353-364. doi:10.1038/nrn1104

35. Wolak DJ, Thorne RG. Diffusion of macromolecules in the brain: Implications for drug delivery. *Mol Pharm*. 2013;10(5):1492-1504. doi:10.1021/mp300495e

36. Pizzo ME, Wolak DJ, Kumar NN, et al. Intrathecal antibody distribution in the rat brain: surface diffusion, perivascular transport and osmotic enhancement of delivery. *J Physiol*. 2018;596(3):445-475. doi:10.1113/JP275105

37. Davson H, Segal MB. *Physiology of the CSF and Blood-Brain Barriers*. Boca Raton: CRC Press; 1996.

38. Tibbling G, Link H, Öhman S. Principles of albumin and igg analyses in neurological disorders. I. Establishment of reference values. *Scand J Clin Lab Invest*. 1977;37(5):385-390. doi:10.1080/00365517709091496

39. Link H, Tibbling G. Principles of albumin and igg analyses in neurological disorders. II. Relation of the concentration of the proteins in serum and cerebrospinal fluid. *Scand J Clin Lab Invest*. 1977;37(5):391-396. doi:10.1080/00365517709091497

40. Jesse S, Brettschneider J, Süssmuth SD, et al. Summary of cerebrospinal fluid routine parameters in neurodegenerative diseases. *J Neurol*. 2011;258(6):1034-1041.

doi:10.1007/s00415-010-5876-x

41. Thorne RG, Nicholson C. In vivo diffusion analysis with quantum dots and dextrans predicts the width of brain extracellular space. *Proc Natl Acad Sci U S A*. 2006;103(14):5567-5572. doi:10.1073/pnas.0509425103

42. Novak U, Kaye AH. Extracellular matrix and the brain: Components and function. *J Clin Neurosci*. 2000;7(4):280-290. doi:10.1054/jocn.1999.0212

43. Wolak DJ, Thorne RG. Diffusion of macromolecules in the brain: Implications for drug delivery. *Mol Pharm*. 2013;10(5):1492-1504. doi:10.1021/mp300495e

44. Somjen GG. *Ions in the Brain: Normal Function, Seizures, and Stroke*. New York: Oxford University Press; 2004.

45. Hille B. *Ion Channels of Excitable Membranes*. Sunderland, Massachusetts: Sinauer Associates, Inc; 2001.

CNS disorder	Intervention	Target	Phase
spinal muscular atrophy	nusinersen	SMN2	approved
amyotrophic lateral sclerosis (ALS)	tofersen	SOD1	phase 3
Huntington's disease	RG6042 (HTT_{RX})	HTT	phase 3
Alzheimer's disease & frontotemporal dementia	$MAPT_{RX}$	tau	phase 2
amyotrophic lateral sclerosis (ALS)	IONIS-$C9_{RX}$	C9ORF72	phase 2
Huntington's disease	WVE-120101	mHTT (SNP1)	phase 1/2
Huntington's disease	WVE-120102	mHTT (SNP2)	phase 1/2
centronuclear myopathy	IONIS-DNM2-2.5_{RX}	DNM2	phase 1
Parkinson's disease	ION859	LRRK2	phase 1

Table 1: Antisense oligonucleotides currently approved or in clinical trials for central nervous system disorders

CHAPTER 3
Factors influencing therapeutic antisense oligonucleotide distribution in the CNS following intrathecal administration

Brynna Wilken-Resman[1], Michelle E. Pizzo[1,2], Charles Lauhon[1], and Robert G. Thorne[1,2]
[1]School of Pharmacy, Division of Pharmaceutical Sciences; University of Wisconsin-Madison, Madison, Wisconsin, USA [2]Denali Therapeutics, San Francisco, California, USA

Abstract

This chapter describes studies investigating how antisense oligonucleotide (ASO) therapeutics administered via the intrathecal route into the cerebrospinal fluid in rats reach their targets in cortical and subcortical regions and how they are cleared from the CNS. ASO biodistribution in the CNS was consistent with parenchymal diffusion and more complex transport in other compartments: A diffusive gradient was observed at CSF-brain interfaces along with prominent ASO signal within the perivascular spaces surrounding blood vessels of varying caliber. Comparison of the biodistribution of different ASO chemistries with similar molecular weight and charge suggests that factors including nucleotide sequence and chemical modification can interact with unique physiological and anatomical features of the brain and spinal cord to significantly impact the resulting CNS distribution of intrathecally infused ASO therapeutics. Use of integrative optical imaging diffusion measurements to evaluate ASO-protein interactions suggests that the modified phosphorothioate linkage typical of ASOs currently used clinically facilitates binding with protein in the cerebrospinal fluid (CSF), leading to an increase in the apparent size of the ASO.

Introduction

Antisense oligonucleotide (ASO) therapeutics are single stranded DNA or RNA oligonucleotides, typically with a negatively-charged backbone, that belong to a drug class with the potential to treat disorders for which the genetic cause is known. ASOs interfere with the normal translation of RNA into protein via several mechanisms that can block the production of an unwanted or toxic protein or allow or modify the production of a desired protein.[1,2] Commercial success was achieved recently, with approvals for ASO therapeutics targeting

peripheral disorders including mipomersen (Kynamro) in 2013 for homozygous familial hypercholesterolemia[3], eteplirsen in 2016 for Duchenne muscular dystrophy[4], and inotersen in 2018 for hereditary transthyretin amyloidosis. [5] The pace of ASO approval has increased rapidly in part due to chemical modifications that have improved their systemic pharmacokinetics and binding affinity to target RNA.[6,7] However, the development of ASO therapeutics for CNS disorders has been significantly complicated by the presence of CNS barriers that impede paracellular transport from the plasma to brain and spinal cord targets. Brain capillary endothelial cells forming the blood-brain barrier (BBB) arguably represent the most important of these barriers; BBB tight junctions, adherens junctions and efflux transporters effectively prevent large, charged molecules such as ASOs from entering the brain parenchyma from the blood[7–9], making common routes of administration such as intravenous infusion impractical. This has motivated the clinical pairing of ASOs targeting certain neurological diseases with central delivery methods that bypass the blood-brain barrier, specifically intrathecal administration into the CSF. Intrathecal administration of nusinersen, an ASO that alters the splicing of *spinal motor neuron 2* pre-RNA to increase expression of the SMN protein, was approved in 2016 for the treatment of spinal muscular atrophy, a disease with targets primarily in spinal motor neurons. [10,11] Clinical trials are ongoing for intrathecal ASO therapy against other targets for Huntington's disease, amyotrophic lateral sclerosis (ALS), Alzheimer's disease, and frontotemporal dementia, among others.[2] Surprisingly, it is not well understood how these intrathecally-administered ASO therapeutics reach their targets in cortical and subcortical regions of the CNS and how they exit the CNS. Furthermore, it's yet unclear if the chemistries and modifications on the ASOs that were successful in treating diseases in the periphery are also the optimal chemistries and modifications to treat disorders affecting the central nervous system. The brain and spinal cord

have a unique environment and physiology that should be considered for development and optimization of ASOs to treat neurological disorders.

Intrathecal administration consists of direct infusion or injection into the CSF of the lumbar spinal cord or the cisterna magna. The CSF into which ASOs are administered is continuous with the subarachnoid space that surrounds the brain and spinal cord. Convection or bulk flow of CSF and CSF-borne solutes is thought to occur in the subarachnoid space. [12,13] Solutes in the subarachnoid space CSF, including infused macromolecules, are not immediately in contact with the brain parenchyma, but are separated by the innermost meningeal layer (pia mater), as well as a layer of astrocytic foot processes (glia limitans) which may hinder or restrict macromolecule entrance at the subarachnoid space-brain interface. [14]

Diffusion is often stated or implied as the mechanism by which ASOs access CNS tissues after intrathecal administration[15–17], provided a mechanism of distribution is mentioned. Coronal brain sections examined after ASO or other macromolecule tracer administration into the CSF have demonstrated a gradient at the CSF-brain interfaces[18,19] consistent with diffusion. Intrathecally-infused macromolecules in the subarachnoid space CSF first cross the pia mater and the glia limitans before reaching the brain parenchyma where they can move through the brain's extracellular spaces (ECS). The ECS in the brain has previously been shown to be approximately 40-60 nm in width[20]. The ECS dimensions are thought to be too narrow to allow for convective or bulk flow via the ISF, [13,21–23] therefore movement of ASOs or other macromolecules in the ECS under normal conditions has been thought to be dominated by diffusion, or random mixing of solute driven by the concentration gradient. [24] The steady state concentration (C) in the tissue

at any distance (x) from the concentration in the CSF at the brain surface (C_0) is given by the solution to Fick's second law[25,26] (known as the macroscopic diffusion equation):

$$\frac{C}{C_0} = e^{-x(k_e/D^*)^{1/2}} \qquad \text{Equation 1}$$

where D^* is the effective diffusion coefficient in brain, and k_e is the efflux constant. The diffusion coefficient in brain is macromolecule-specific and dependent on properties that can increase path length to travel around cellular obstacles as well as increase interaction with extracellular components. These properties can include the macromolecule's size, charge, and capacity for binding. [25] ECS volume fraction is conserved among species [27] (i.e. diffusion does not scale with brain size[28]), so the ability of macromolecules to reach deeper brain regions becomes increasingly difficult in species with larger brains.

Perivascular spaces (PVS), fluid and connective-tissue filled compartments surrounding blood vessels, were first identified in the brain in the mid-1800s. In addition to 'perivascular spaces', these spaces have also been referred to as Virchow-Robin spaces or, more recently, as paravascular spaces. [29–31] Indeed, the precise definition of the PVS has been a topic of debate over time but consensus is settling on the idea that the PVS may include the vascular connective tissue space (analogous to the vessel wall tunica adventitia) as well as the basement membrane associated with the smooth muscle cells (analogous to the tunica media). [32] The PVS surrounding the large diameter surface blood vessels (leptomeningeal vessels) in the subarachnoid space can be up to ~5-10 μm wide in rodents, [33,34] which is thought to be large enough to allow for convection or bulk flow within this perivascular compartment due to decreased hydraulic resistance as compared with the narrow brain extracellular spaces. [25] This aspect of the PVS makes it a relevant and potentially scalable conduit for rapid drug delivery to cortical and

subcortical brain regions. The PVS has previously been shown accessible to exogenous macromolecules and tracers that were administered into the CSF.[31,33,35,36] It therefore represents a second potential mechanism of distribution in addition to diffusion for macromolecules administered into the CSF. Recent work reveals that this space may extend throughout the vascular tree to the microvessel or capillary level based on results that show that the parenchymal (astrocyte) and vascular (endothelial) basement membranes are not fused at the level of the capillary [37] as well as reports that show fluorescently-labeled macromolecule tracer surrounding the endothelial layer of microvessels. [35,36] Whether ASOs are also able to access and distribute via the PVS to reach their targets in the CNS and to what extent as well as how ASO chemistries or modifications may affect the transport mechanisms and CNS distribution patterns has rarely been examined in the literature. [19] Improved understanding of ASO transport mechanisms within the unique CNS environment and the interaction of ASO characteristics (e.g. size, charge, nucleotide sequence, chemical modifications) with brain anatomical and physiological features may help inform ASO therapeutic development to enhance efficacy in treating neurological disorders.

Materials and methods

Ethical approval

Experiments were conducted in accordance with the National Institutes of Health Guide for the Care and Use of Laboratory Animals and local Institutional Animal Care and Use Committee regulations. Animals had access to food and water *ad libitum* and were housed in a climate-controlled room with a 12:12 h light/dark cycle. Experiments were terminal and all efforts were made to minimize animal pain and distress.

Cisternal intrathecal infusion in rats and CSF withdrawal

Sprague-Dawley rats (female; 180-270 g; ~10-20 weeks of age; Envigo, Indianapolis, IN, USA) were anesthetized with urethane (1.2 g/kg I.P.) and received supplementary doses (0.375 g/kg) until a surgical plane of anesthesia was reached, as demonstrated by the absence of pedal or palpebral reflexes. Atropine sulfate (0.1 mg/kg S.C. every 2 h) was administered to reduce bronchial secretions. Body temperature was maintained at 37 °C using a homeothermic blanket system (Harvard Apparatus, Holliston, MA, USA). Rats were tracheotomized and an analgesic was administered, 2 % lidocaine hydrochloride (0.05 mL S.C. at the scalp). Rats were then placed in a stereotaxic frame (Stoelting Co., Wood Dale, IL, USA). Cisternal infusion was performed as detailed previously. [36] Briefly, an incision was made along the midline of the scalp and dorsal neck and the underlying posterior vertebral muscles on the back of the neck were then retracted to expose the atlanto-occipital membrane, which was carefully removed from on top of the dura overlying the cisterna magna. A small hole was carefully punctured in the dura with a 30-G dental needle and a cannula was inserted (1.5 cm 33-G polyetheretherketone, PEEK; Plastics One Inc., Roanoke, VA, USA) connected to tubing (PE-10; Solomon Scientific, San Antonio, TX, USA) leading to a Hamilton Syringe controlled by an infusion pump. The cannula was advanced 1 mm into the cisterna magna and cyanoacrylate was used to seal the cannula in the dura and fix it in place. Tubing and syringe were pre-filled with the infusate (80 µL fluorescently labeled ASO) and the 50 min infusion commenced. An infusion rate of 1.6 µL/min was chosen because it is approximately half the cerebrospinal fluid secretion rate in the rat[38] and has been shown to not increase intracranial pressure. [39] After the infusion, the rat was placed supine and the abdominal aorta was cannulated. The animal was then euthanized 30 min post-

infusion by exsanguination via perfusion with 50 mL ice-cold 0.01 M PBS (pH 7.4) at 15 mL/min, followed by perfusion with 4% paraformaldehyde (PFA) in 0.1 M phosphate buffer.

Rat CSF for diffusion experiments was obtained from cisternal puncture. The procedure to puncture the dura and place tubing in the cisterna magna was performed as described for cisternal intrathecal infusion with the substitution of a withdrawal of CSF in place of an infusion. A total of 240 µL of CSF was withdrawn at a rate of 5 µL/min.

Antisense oligonucleotide purchase and preparation

ASOs were purchased from IDT and Midland. ASOs purchased from IDT were fluorescently labeled with AlexaFluor488 and ASOs purchased from Midland were fluorescently labeled with DyLight488. Both fluorescent labels were covalently attached at a 1:1 ratio on the 5' end of the oligonucleotide and added relatively little (<10%) to the overall molecular weight of the ASO. ASOs were received as lyophilized powder, reconstituted with 0.01 M PBS to a concentration of 150 µM, and stored at -20 °C until time of use. Two different ASOs were used, referred to in this paper as 'PS-ASO' and '2'MOE-ASO'. The ASO referred to as 'PS-ASO' is a 19-mer containing the phosphorothioate modification for all linkages between nucleosides. The nucleotide sequence for the PS-ASO is as follows, from 5' to 3': C*G*C*C*G*C*T*G*C*T*G*G*G*G*C*C*A*T*G. The asterisk symbol (*) represents a phosphorothioate internucleoside linkage. The fluorescent label used for the PS-ASO was either DyLight488 or AlexaFluor488. There was no significant difference in hydrodynamic diameter and the CNS distribution appeared indistinguishable between the PS-ASOs with the DyLight or the AlexaFluor label. The ASO referred to as '2'MOE-ASO' is a 20-mer gapmer with the

2’MOE modification (O-methoxy-ethyl modification at the 2’ position on a ribose ring) on the 5’ and 3’ wing segments and the central ‘gap’ region containing phosphorothioate internucleoside linkages. All 2’MOE-ASOs contained the AlexaFluor488 label. The nucleotide sequence for the 2’MOE-ASO is as follows, from 5’ to 3’: c*tcag*T*A*A*C*A*T*T*G*A*C*acca*c. The asterisk symbol (*) represents a phosphorothioate internucleoside linkage. The linkages connecting the rest of the nucleosides are phosphodiester. Capital letters indicate deoxyribose nucleosides, whereas lower case letters indicate 2’-O-methoxyethyl nucleosides. In this case, C and c represent 5-methylcytosine.

Mannitol preparation and co-infusion

D-Mannitol was prepared at 0.75 M in 0.01 M PBS. Osmolarity was measured using an osmometer. Osmolarity of prepared solutions was 1100 to 1110 mOsm. The mannitol solution then replaced the PBS as the solvent for the ASO solution via buffer exchange. ASO in PBS (150 µM) was added to an Amicon filter tube (3 kDa MW cutoff; Millipore, Billerica, MA, USA) along with 0.75 M mannitol. The filter tube was then spun 40 min at 14,000 *g*, a process which was repeated 3 times followed by a recovery spin of 2 min at 1000 *g*. The concentration of the ASO in mannitol after filtration was matched to the concentration of ASO in PBS before filtration by measuring nucleic acid absorbance at 260 nm using a NanoDrop 200C (Thermo Fisher Scientific Inc., Waltham, MA, USA) and adjusting the concentration by adding small volumes of the mannitol solution until the concentration of ASO in mannitol was identical to the concentration of ASO in PBS.

Ex vivo *fluorescence imaging and image processing*

Brain, spinal cord, superficial and deep cervical lymph nodes, and nasal passages were removed and immediately imaged using a MVX10 Macroview microscope (Olympus, Tokyo, Japan) fitted with an X-Cite-120Q illuminator (Lumen Dynamics Group, Inc., Mississauga, Ontario, Canada), an Orca-flash 2.8 CMOS camera (Hamamatsu, Hamamatsu City, Japan) and a FITC filter (Chroma, U-M49002XL, Bellows Falls, VT, USA). Whole brain, spinal cord, and nasal passages were each imaged at a series of different planes of focus for multiple overlapping sections. Planes of focus were autoblended and overlapping sections were aligned manually in Photoshop CC (Adobe Systems, San Jose, CA, USA) to create a single image. The brain and rostral cervical spinal cord were sectioned coronally at a thickness of 100 µm using a vibratome (VT1000S; Leica Microsystems, Wetzlar, Germany) and imaged using the MVX10 for detection of the fluorescently labeled ASO.

Immunohistochemistry and confocal imaging

Free-floating coronal sections were blocked for 1 hour in 5% goat or donkey serum or 2.5 % goat and 2.5 % donkey serum in 0.01 M PBS with 0.03 % Triton-X. Sections were then incubated overnight at 4 °C with primary antibody in blocking buffer. Primary antibodies and dilutions used include: rat endothelial cell antigen-1 (RECA-1; ab9774; Abcam, Cambridge, MA, USA; dilution 1:1000), rabbit-anti-NeuN (ab177487; Abcam, Cambridge, MA, USA; dilution 1:500), chicken-anti-GFAP (NBP1-05196; Novus Biologicals, Littleton, OH, USA; dilution 1:1000), goat-anti-Iba-1 (NB100-1028; Novus Biologicals; dilution 1:100), and mouse-anti-laminin γ1 (mab 2139; R&D Systems, Minneapolis, MN, USA; dilution 1:500). Sections were then washed in ice cold PBS 3 times for 15 min each and incubated for two hours at room temperature in

secondary antibody solution in blocking buffer at a dilution of 1:500. Secondary antibodies used include: goat-anti-mouse 647 (ab150119; Abcam), donkey anti-mouse 647 (ab150107; Abcam), goat anti-rabbit 594 (A11012; Life Technologies, Eugene, OR, USA), goat-anti-chicken 594 (ab150172; Abcam), and donkey-anti-goat 546 (A11058; Life Technologies). Sections were then washed again in PBS and incubated for 20 min at room temperature with DAPI (Life Technologies; dilution 1:1000) and washed 3 more times in PBS before mounting on slides using Prolong Diamond Antifade (Life Technologies). Slides were imaged on an A1R confocal microscope with NIS Elements (Nikon, Tokyo, Japan).

Diffusion measurements in free medium using integrative optical imaging

We measured the free diffusion of the ASOs using the integrative optical imaging (IOI) method, as described previously. [20,26,28,40] Fluorescently-labeled ASOs were pressure-ejected from a glass micropipette (tip diameter 5-10 μm) (catalog 617000, A-M Systems, Carlsborg, WA, USA) into a medium of 0.3 % NuSieve GTG agarose (FMC, Philadelphia, PA, USA), maintained at 37.0± 0.5 °C. Diffusion of the ASOs was imaged at 1 second intervals using epifluorescence microscopy. Ejection volume was approximately 25-50 pL, resulting from a 100-millisecond pulse of nitrogen (Toohey Spritzer, Toohey, Fairfield, NJ, USA), approximating a point source. Epifluorescence microscopy equipment consists of an Olympus BX61WI microscope equipped with a water-immersion objective (UM PlanFl 10x, NA 0.3; Olympus, Center Valley, PA, USA), Fluorescein isothiocyanate (FITC) filter set (Chroma, Bellows Falls, VT, USA), and a CCD camera (Cool-Snap HQ^2; Photometrics, Tucson, AZ, USA). The following equations describe how the 3D diffusion images are projected onto the camera, the theory of which is described elsewhere[26,40]:

$$I_i(r, \gamma_i) = E_i \exp\left[-(r/\gamma_i)^2\right] \quad \text{Equation 2}$$

and

$$\gamma_i{}^2 = 4D(t_i + t_0) \quad \text{Equation 3}$$

where I_i represents the intensity of the *i*th image at a distance, *r*, from the injection point and E_i represents the defocused point spread of the microscope objective. Fluorescence intensity curves were extracted from the diffusion images along six axes. Equation 2 was fit to the upper 90 % of the resulting intensity curves using a nonlinear simplex algorithm in a custom MatLab program. Fits returned estimates for a parameter, γ_i, at a time interval (t_i) after injection approximating a point source (t_0). The free diffusion coefficient (*D*) was obtained from linear regression using Equation 3. The highest and lowest of the *D* values obtained along the six axes were discarded and the average *D* was calculated. The apparent hydrodynamic diameter (d_H) was then calculated from the Stokes-Einstein equation and the average *D* value:

$$d_H = (kT)/(3\pi\eta D) \quad \text{Equation 4}$$

where *k* is Boltzmann's constant, *T* is absolute temperature, and η is the viscosity of water (6.9152×10^{-4} Pa s at $T = 310$ K).

Perivascular quantification

Fluorescent perivascular signal after intrathecal infusion of ASO was quantified using Fiji,[41] adapted from the method previously described in detail. [36] Two coronal levels were selected: ~1 mm anterior to bregma (eight sections per animal), and ~5.5 mm posterior to bregma (eight sections per animal). [42] A wand tool was used to select the area of the coronal section (ventricles were excluded from the sections centered around +1 mm, and the region of interest selected for sections centered around -5.5 mm was the posterior hippocampus. Coronal sections from the

more +1 mm were split into dorsal and ventral regions for the purpose of quantification due to the regional heterogeneity in signal. The fluorescent signal remaining after uniformly adjusting the brightness to remove autofluorescence was then quantified by the "analyze particles" command. Quantification was reported as "percent area" and/or "counts per mm", referring to the percentage of the total slice area that was occupied by signal from the fluorescent probe including perivascular signal and diffuse surface/white matter signal, or the number of fluorescent puncta observed per millimeter of brain tissue, respectively.

Statistical analysis

All values are reported as mean ± standard error (SE). Student's t-test (unpaired) was used to determine statistical significance for all two-way comparisons, with corresponding p values found in the text. The difference between two groups was determined to be statistically significant where $p < 0.05$. One-way ANOVA with post-hoc Holm-Sidak test was used for data requiring multiple comparisons, except where noted due to deviations from normality in the data. Statistical analyses were performed using SigmaPlot (San Jose, CA, USA).

Results

Whole brain ex vivo *fluorescence imaging*

Ex vivo fluorescence imaging following demonstrated perivascular transport of ASOs. Following intrathecal infusion in rats, perfused and fixed brains were removed and imaged for detection of fluorescence indicating ASO presence. Signal was found on the dorsal and ventral brain surfaces surrounding the cerebral blood vessels. This was especially apparent on the ventral surface, with a high amount of signal in the perivascular spaces surrounding major arteries, including the

vertebral, basilar, and middle cerebral arteries as well as vasculature comprising the circle of Willis. Signal was mainly restricted to the perivascular spaces surrounding major ventral arteries for the PS-ASO alone and with hyperosmolar mannitol (Figure 1A and 1B) whereas 2'MOE-ASO signal appeared more diffuse along the dorsal and ventral surfaces (Figure 1C). Punctate signal corresponding to smaller penetrating vessels perpendicular to the brain surface can also be seen on both the dorsal and ventral surfaces for both PS-ASO and 2'MOE-ASO but was more prominent for 2'MOE-ASO.

Ex vivo *fluorescence imaging of coronal brain sections*

Coronal sections were cut and imaged, allowing an overview of the distribution of the fluorescent probe along the neural axis from the olfactory bulbs to the cervical spinal cord (Figure 2 A-O). Two distinct types of distribution were observed upon imaging of coronal brain sections: a diffusive gradient at the CSF-brain interface at the pial surface and punctate perivascular profiles in the brain parenchyma. In animals infused with 2'MOE-ASO, strong fluorescent signal was frequently observed in periventricular white matter tracts (Figure 2L).

The increase in fluorescent signal in coronal brain sections for the 2'MOE-ASO compared with the PS-ASO alone and the PS-ASO co-infused with hyperosmolar mannitol is apparent not only visually but was also quantified using Fiji/ImageJ. Signal quantification revealed that the fluorescent signal as a percent of total area was significantly higher for 2'MOE-ASO when compared with PS-ASO alone and PS-ASO with mannitol for a region of interest centered at 1 mm anterior to bregma (Figure 2P). This may be partially due to increased diffusion and periventricular white matter signal observed in the animals infused with 2'MOE-ASO as well as

increased perivascular signal. Fluorescent counts per square millimeter is a second measure for quantifying signal in coronal sections. It is particularly useful for counting fluorescent puncta resulting from vessels running perpendicular to the tissue section. Results from measuring fluorescent counts for the dorsal half of the same coronal sections revealed that there was significantly higher punctate signal associated with perivascular spaces for the animals receiving 2'MOE-ASO when compared with the animals receiving PS-ASO alone and PS-ASO with mannitol, in agreement with the results from the percent area measurement (Figure 2Q). Counts normalized to area could not be accurately quantified for the ventral halves due to diffuse signal at the ventral surface obscuring perivascular signal. Similar results were obtained using sections centered at 5.5 mm posterior to bregma where the region of interest for quantification was the posterior hippocampus, chosen because it is a subcortical structure with consistent fluorescent perivascular signal. 2'MOE-ASO had significantly more fluorescent counts per square millimeter compared with PS-ASO alone and PS-ASO with mannitol (Figure 2R).

Co-infusion of hyperosmolar mannitol is a method that has previously been used to enhance perivascular access of IgG in a rat model.[36] It was hypothesized that hyperosmolar mannitol in the subarachnoid space CSF could draw water out of cells lining the leptomeningeal blood vessels, potentially increasing gaps between cells and increasing the size of pores or stomata on the leptomeningeal cells to allow greater access to the PVS. However, the PS-ASO co-infusion with mannitol did not reveal a statistically significant difference from PS-ASO alone by either quantification measure (fluorescent signal as a percent of total area or fluorescent counts per square millimeter) or at either bregma level studied (+1 mm and -5.5 mm) (Figure 2P-R).

Fluorescent signal associated with perivascular spaces surrounding arterioles, venules, and vessels of differing caliber

Perivascular signal was found around both arterioles (Figure 3A and 3B) and venules (Figure 3B and 3C) as well as in microvessels with a diameter of around 10 μm or less (Figure 3H and 3I). PS-ASO and 2'MOE-ASO distributed dissimilarly within different compartments of the perivascular space. While both ASOs accessed the vascular connective tissue space of the vessel wall (tunica adventitia), the PS-ASO appeared to have restricted access to the smooth muscle basement membrane (tunica media) (Figure 3E) compared to the 2'MOE-ASO (Figure 3G). Addition of mannitol did not appear to have an impact on the ability of the PS-ASO to access the smooth muscle layer of arterioles (Figure 3F).

Internalization

Cell uptake of the fluorescently labeled ASOs is visible in cells (neuronal and non-neuronal) nearby vessels with perivascular ASO signal and at CSF-brain interfaces, as shown by colocalization of ASO with the nuclear marker, DAPI, and/or the neuronal marker, NeuN (Figure 3B, 3I, 3J).

ASO size and effects of sequence and chemical modification on ASO binding to CSF protein

Diffusion coefficients measured from IOI experiments revealed that the fluorescently labeled PS-ASO (6.8 kDa) had a diffusion coefficient of $1.51 \pm 0.06 \times 10^{-6}$ cm^2s^{-1} (n=15) and, related by the Stokes-Einstein equation, an apparent hydrodynamic diameter of 4.36 ± 0.18 nm. The fluorescently labeled 2'MOE-ASO (7.8 kDa) had a diffusion coefficient of $2.13 \pm 0.05 \times 10^{-6}$ cm^2s^{-1} (n=14) and an apparent hydrodynamic diameter of 3.09 ± 0.07 nm. Comparison of PS-

ASO and 2'MOE-ASO apparent size reveals that the PS-ASO is ~40 % larger than the 2'MOE-ASO. When rat CSF was mixed with each ASO, the apparent hydrodynamic diameter increased to 5.19 ± 0.17 nm for the PS-ASO (n=10), whereas the slight increase in apparent hydrodynamic diameter was not statistically significant for the 2'MOE-ASO (3.30 ± 0.05 nm, *n*=11). CSF concentration of albumin (approximately 150 mg/L, or 2.3 μM) mixed with PS-ASO similarly produced a larger apparent hydrodynamic diameter for the PS-ASO in this mixture (4.97 ± 0.12 nm, *n*=11) compared to PS-ASO alone. This value was not statistically different from PS-ASO mixed with CSF. CSF concentration of albumin mixed with 2'MOE-ASO yielded no significant change in apparent hydrodynamic diameter of the 2'MOE-ASO in this mixture (3.14 ± 0.13 nm, *n*=9) compared to 2'MOE-ASO alone or 2'MOE-ASO mixed with CSF. Plasma concentration of albumin (650 μM) mixed with ASO produced significantly larger apparent hydrodynamic diameters for both PS-ASO (7.39 ± 0.38 nm, n=5) and 2'MOE-ASO (3.86 ± 0.12 nm, n=13) compared to the respective ASOs alone or mixed with CSF or CSF concentrations of albumin. Comparison of apparent hydrodynamic diameters can be found in Figure 4.

CSF clearance via the olfactory drainage pathway

The presence of fluorescent signal in the nasal passages (Figure 5A and 5B) suggested that ASO drained from the CNS at least in part via an olfactory pathway. The olfactory mucosa as well as the deep cervical lymph nodes consistently displayed fluorescent signal following intrathecal administration for all groups tested (PS-ASO, 2'MOE-ASO, and PS-ASO with mannitol). Fluorescent signal was also noticeable along the olfactory nerve layer (Figure 2K) and at the cribriform plate. Fluorescent signal in superficial cervical lymph nodes was only occasionally present (data not shown), and when present it was of lower intensity compared to the signal in

the deep cervical lymph nodes (Figure 5C and 5D). These results which indicated an olfactory drainage pathway for ASOs are consistent with observations made for intrathecally-infused IgG[36] as well as radiolabeled human serum albumin and Evans blue-labeled albumin after intracerebral injection.[43]

Discussion

This study involved two ASOs with differences not only in chemistry but also nucleotide sequence, therefore the objective of this study was to highlight the dramatic difference in CNS distribution of two ASOs of similar in molecular weight and charge. We secondarily proposed several factors that could lead to this difference, including ASO size, binding, and electrostatic effects. Given that there are multiple differences between the two ASOs in sequence and chemistry it was not feasible to determine how each individual factor contributed to the difference in distribution. However, what is apparent is that two ASOs, similar in molecular weight and charge and subjected to the same infusion paradigm, differed dramatically in the extent of distribution to CNS tissues.

There is a size-dependent aspect to transport via both diffusion and access to the perivascular space. The effect of particle size on diffusion in the extracellular space is well-known and access to the perivascular space is also thought to be size-dependent. [35,36] The apparent size, d_H, of the PS-ASO was significantly (~40 %) larger than the 2'MOE-ASO despite the PS-ASO's smaller molecular weight (6.8 kDa and 7.8 kDa, respectively). This likely reflected sequence-dependent formation of secondary structure at physiological temperature in the case of the PS-ASO whereas the 2'MOE-ASO, for which the sequence chosen didn't support formation of secondary

structure, appears condensed as a random coil. [44,45] In addition to complementary base pairing, sequence-dependent base stacking may have also impacted the conformation and electrostatic interactions of the ASO. [45–48]

Despite the evidence that the apparent size of the ASO may impact its CNS distribution, it is unlikely to be the sole factor responsible for the difference in distribution of the two ASOs. This point is demonstrated by comparing the distribution of the sdAb[36] to that of the PS-ASO. These two macromolecules, which had similar hydrodynamic diameters and were administered using an identical intrathecal infusion paradigm and fluorescent label, differed dramatically in the extent to which they diffused through the ECS and distribute via the PVS, which suggested that there are additional factors hindering the diffusion and perivascular access of PS-ASO in the CNS.

Electrostatic interactions between the polyanionic ASOs and negatively charged components in the CNS could increase ASO hindrance. Despite both ASOs having a similar charge the PS-ASO may have a farther-reaching electrostatic effect. Its larger apparent size could translate to a larger sphere of electrostatic influence, thereby increasing the likelihood of charge interactions. Due to the narrow ECS width in the CNS and the abundance of ECM components such as proteoglycans with anionic sulfate and carboxyl groups[22,49], the larger sphere of electrostatic influence may be a meaningful source of hindrance in the ECS and within the basement membranes in the PVS.

Protein binding is another possible factor affecting distribution of ASOs in the CNS. The known tendency of ASOs with a phosphorothioate backbone to bind to albumin[50–52] may hinder the

CNS distribution of the PS-ASO. Albumin is typically recognized as playing an important role in binding therapeutics in the periphery. Albumin binding to phosphorothioated ASOs improves the pharmacokinetics of ASOs administered via conventional systemic routes by reducing rapid renal excretion that would otherwise occur. [53] However, albumin's presence in the CSF and in CNS tissues is often dismissed because its CSF concentration is far lower than its plasma concentration; indeed, the effects that CSF and CNS tissue albumin could have on ASO distribution in the brain and spinal cord appears not to have been given serious consideration previously. Due to an increase in apparent size, bound ASO in the subarachnoid space CSF may encounter more difficulty in accessing the PVS through pores and/or intercellular clefts in the large leptomeningeal surface vessels. Our work demonstrated that the PS-ASO (fully phosphorothioated) bound to albumin and increased the apparent size of the ASO even when albumin was present at very low CSF concentrations, which suggested that ASO with a fully phosphorothioated backbone binds non-negligibly to albumin. Importantly, concentrations of albumin and other proteins in the CSF can be dynamic across ages and disease status. Infantile CSF protein concentration is elevated at birth, decreases in the first year of life, remains stable until around age 40, then increases after that point. [38,54] This means that certain patient populations for diseases including spinal muscular atrophy (commonly affecting infants and young children) and Alzheimer's disease and other dementias (typically affecting older adults) have varied concentrations of protein even before accounting for how pathology may affect CSF protein concentration. CSF proteins including albumin are elevated in some neurological disorders[55] including amyotrophic lateral sclerosis (ALS), multisystem atrophy, and progressive supranuclear palsy. [56]

Infusion of 2'MOE-ASO produced fluorescent signal bordering the lateral ventricle, including signal in the corpus callosum directly above the ventricle, suggesting that the 2'MOE-ASO is able to access the CSF of the lateral ventricle, although the mechanism by which this happens is at present unclear. Once in the CSF of the ventricle, the 2'MOE-ASO could diffuse across the ependymal cells lining the ventricles, which lack tight junctions in the adult brain. [57–59] Prominent signal immediately above the lateral ventricle in the corpus callosum white matter could be due to reduced hydraulic resistance as a result of the parallel alignment of axons. Although the precise mechanism is unknown, several potential routes of entry for intrathecally-infused tracers to access the ventricles have been recently hypothesized by Pizzo et al. [36] We do not expect that the 2'MOE-ASO signal observed adjacent to the lateral ventricles or the periventricular white matter is due to backflow from the cisternal infusion. Fluorescent signal due to backflow (i.e. in the opposite direction of CSF flow through the ventricular system) would be most apparent around the 4th ventricle, followed by the 3rd and then the lateral ventricles. However, we do not see substantial fluorescent signal surrounding the 4th or 3rd ventricles. It is interesting to note that PS-ASO signal was rarely found in white matter or tissue adjacent to the lateral ventricles. While previous work with full-length IgG and sdAb (single domain antibody) has been shown to exclude larger molecules from ventricular or periventricular access, size-dependent entry is unlikely to be the only differentiating factor since a sdAb with a similar hydrodynamic diameter as the PS-ASO reliably showed periventricular signal. [36]

Drainage of CSF has traditionally been thought to occur via uptake from the arachnoid projections into the draining venous sinuses in the dura as well as via cranial and spinal nerves, and more recently via dural lymphatics. [60,61] A number of groups, including ours, have

previously published work suggesting an olfactory drainage pathway[36,60,62–65] whereby CSF and tracers in the CSF can cross the cribriform plate via perivascular spaces, cranial nerves, and/or lymphatics to reach the nasal passages, specifically the olfactory mucosa, and subsequently drain via nasal lymphatics to the deep cervical lymph nodes. In the present study, fluorescence microscopy consistently showed high ASO signal at the olfactory nerve layer surrounding the olfactory bulbs, the cribriform plate, the olfactory mucosa, and the deep cervical lymph nodes, consistent with this previous work. These results suggest that ASOs drain, at least in part, via an olfactory route. Superficial cervical lymph nodes rarely contained fluorescent signal, and when they did the signal was dim in comparison to the deep cervical lymph nodes.

The anatomy of the spinal cord may help explain the striking difference in spinal cord distribution between the PS-ASO and 2'MOE-ASO. As opposed to the brain, where the most superficial CSF-brain interface consists of gray matter, the superficial CSF-spinal cord interface consists of white matter, with the cell bodies of motor and sensory neurons located in the gray matter at the interior of the spinal cord. As described previously, the white matter is thought to be a region of lower hydraulic resistance. This may explain the diffuse 2'MOE-ASO signal in the white matter of the spinal cord. The PS-ASO, however, appears less able to cross the pia, resulting in reduced PS-ASO signal in the spinal white matter. Punctate perivascular signal corresponding to vessels traveling perpendicular to the spinal cord section can be seen in some of the spinal cord sections that were examined, although there appears to be variability in this distribution between animals.

There are several variables involved in intrathecal administration that may affect the outcome of therapy. One such variable is body positioning. A variety of patient positions have been used in the clinic, including prone, lateral, and sitting. [66,67] Recent research involving intrathecally administered adeno-associated virus (AAV) therapy for the treatment of spinal muscular atrophy shows that positioning patients in the Trendelenberg position (patient tilted head down) can enhance the efficacy of AAV transduction in the brain because the position ameliorates macromolecules 'settling' caudally along the spinal cord. [68,69] Similarly, it has been suggested that perivascular transport of intrathecally-administered fluorescent tracers in mice may also be affected by body positioning (prone, lateral, or supine)[70] or by anesthesia or sleep versus awake state, although the effect these brain states may have on distribution and clearance of macromolecules in the CSF remains poorly understood[70–72]; a detailed discussion of the possible effects resulting from these many different administration variables has recently been provided by Abbott and colleagues. [73]

Yet another potential variable relevant to the distribution of intrathecal therapeutics could be infusion rate and location. There is not yet a consensus on the most effective infusion rate, and the literature shows a range of intrathecal infusion rates for ASOs, from bolus injections currently favored in the clinic[74–76] to longer infusions [18,77]. A recent study looking at slow versus fast intrathecal administration of recombinant AAVs at the lumbar subarachnoid space showed better transduction efficiency in the spinal cord tissue with a slow infusion rate but a better transduction efficiency in brain tissue with a faster infusion rate. [78] Whether this pattern would hold true for other macromolecule therapeutics such as ASOs has yet to be proven. Cellular internalization of ASOs may also be affected by infusion rate, as it has been proposed that bolus

injection may lead to more efficient ‘productive’ uptake pathways in the cell. [74] The location of the administration may play a role in ASO distribution. It should be noted that the present study examines intrathecal administration into the subarachnoid space of the cisterna magna whereas intrathecal administration in the clinic is most typically performed in the subarachnoid space at the level of the lumbar spinal cord, which is a safer location but further from therapeutic target sites in the brain. Lumbar intrathecal administration also presents additional complications in understanding flow patterns and microanatomical features that may impact CSF flow and mixing in the spinal subarachnoid space. [79] There is also interest in intracerebroventricular (ICV) administration (injection or infusion into the CSF-filled lateral ventricle) for macromolecule therapeutics. Interest in the ICV route has primarily been stimulated by recent experiences with protein therapeutics[80] including an FDA-approved enzyme replacement therapy, cerliponase alfa, for CLN2 disease. [81] Although there are benefits and limitations to ICV administration, the location of ICV infusion at the CSF of the brain as opposed to the spinal cord presents an interesting opportunity to potentially achieve a different pattern of distribution in the brain. It is beyond the scope of this paper to address these variables to intrathecal ASO therapy in depth, but it is important to recognize that they may play an important role in achieving the best possible CNS delivery of ASOs and other macromolecule therapeutics. In order to understand how these variables may further enhance CNS distribution of ASOs, it is crucial to have a strong understanding of ASO transport mechanisms and how ASOs interact with the unique physiology and anatomy of the brain.

Overall, this study was intended to provide a thorough examination of ASO distribution in the central nervous system after intrathecal administration. Our results show that limited diffusion

occurs at the CSF-brain interface and that access to the perivascular spaces is important for ASO delivery to cortical and subcortical regions that are target sites for many neurological disorders. The dramatic difference in perivascular signal and diffusion at the CSF-brain interface further indicates that ASO distribution in the brain and spinal cord is highly dependent on factors specific to each ASO. These factors include hydrodynamic size, electrostatic interactions, and binding to components in the CSF and CNS. Nucleotide sequence and chemical modification can affect these factors in interrelated ways and could potentially be used as tools to enhance or tune ASO distribution in the CNS. Further research is needed to explore each factor to draw firmer conclusions regarding the relative contributions of each individual factor to the CNS distribution of the ASO. ASOs intended for CNS disorders clearly need to be optimized for CNS delivery, which may be different than those optimal for treatment of peripheral disorders due to the unique CNS anatomy and physiology.

1. Bennett CF, Swayze EE. RNA Targeting Therapeutics: Molecular Mechanisms of Antisense Oligonucleotides as a Therapeutic Platform. *Annu Rev Pharmacol Toxicol*. 2010;50(1):259-293. doi:10.1146/annurev.pharmtox.010909.105654

2. Rinaldi C, Wood MJA. Antisense oligonucleotides: The next frontier for treatment of neurological disorders. *Nat Rev Neurol*. 2018;14(1):9-22. doi:10.1038/nrneurol.2017.148

3. Hair P, Cameron F, McKeage K. Mipomersen sodium: First global approval. *Drugs*. 2013;73(5):487-493. doi:10.1007/s40265-013-0042-2

4. Aartsma-Rus A, Krieg AM. FDA Approves Eteplirsen for Duchenne Muscular Dystrophy: The Next Chapter in the Eteplirsen Saga. *Nucleic Acid Ther*. 2016;27(1):1-3. doi:10.1089/nat.2016.0657

5. Keam SJ. Inotersen: First Global Approval. *Drugs*. 2018;78(13):1371-1376. doi:10.1007/s40265-018-0968-5

6. Geary RS, Watanabe TA, Truong L, et al. Pharmacokinetic Properties of 2 J - O - (2-Methoxyethyl) -Modified Oligonucleotide Analogs in Rats. *J Pharmacol Exp Ther*. 2001;296(3):890-897.

7. Geary RS, Norris D, Yu R, Bennett CF. Pharmacokinetics, biodistribution and cell uptake of antisense oligonucleotides. *Adv Drug Deliv Rev*. 2015;87:46-51. doi:10.1016/j.addr.2015.01.008

8. Banks WA, Farr SA, Butt W, Kumar VB, Franko MW, Morley JE. Delivery across the blood-brain barrier of antisense directed against amyloid beta: reversal of learning and memory deficits in mice overexpressing amyloid precursor protein. *J Pharmacol Exp Ther*. 2001;297(3):1113-1121. http://www.ncbi.nlm.nih.gov/pubmed/11356936.

9. Agrawal S, Temsamani J, Tang JY. Pharmacokinetics, biodistribution, and stability of oligodeoxynucleotide phosphorothioates in mice. *Proc Natl Acad Sci U S A*. 1991;88(17):7595-7599. doi:10.1073/pnas.88.17.7595

10. Bennett CF. Therapeutic Antisense Oligonucleotides Are Coming of Age. *Annu Rev Med*. 2019;70(1):307-321. doi:10.1146/annurev-med-041217-010829

11. Scoles DR, Minikel E V., Pulst SM. Antisense oligonucleotides: A primer. *Neurol Genet*. 2019;5(2). doi:10.1212/NXG.0000000000000323

12. Papisov MI, Belov V V., Gannon KS. Physiology of the intrathecal bolus: The leptomeningeal route for macromolecule and particle delivery to CNS. *Mol Pharm*. 2013;10(5):1522-1532. doi:10.1021/mp300474m

13. Davson H, Segal MB. *Physiology of the CSF and Blood-Brain Barriers*. 1st ed. Boca Raton: CRC Press, Inc; 1995.

14. Ghersi-Egea JF, Finnegan W, Chen JL, Fenstermacher JD. Rapid distribution of intraventricularly administered sucrose into cerebrospinal fluid cisterns via subarachnoid velae in rat. *Neuroscience*. 1996;75(4):1271-1288. doi:10.1016/0306-4522(96)00281-3

15. Wild EJ, Tabrizi SJ. Therapies targeting DNA and RNA in Huntington's disease. *Lancet*

Neurol. 2017;16(10):837-847. doi:10.1016/S1474-4422(17)30280-6

16. Wild EJ, Tabrizi SJ. Targets for future clinical trials in Huntington's disease: What's in the pipeline? *Mov Disord*. 2014;29(11):1434-1445. doi:10.1002/mds.26007

17. Evers MM, Toonen LJA, van Roon-Mom WMC. Antisense oligonucleotides in therapy for neurodegenerative disorders. *Adv Drug Deliv Rev*. 2015;87:90-103. doi:10.1016/j.addr.2015.03.008

18. Kordasiewicz HB, Stanek LM, Wancewicz E V., et al. Sustained Therapeutic Reversal of Huntington's Disease by Transient Repression of Huntingtin Synthesis. *Neuron*. 2012;74(6):1031-1044. doi:10.1016/j.neuron.2012.05.009

19. Yee F, Ericson H, Reis DJ, Wahlestedt C. Cellular uptake of intracerebroventricularly administered biotin- or digoxigenin-Labeled antisense oligodeoxynucleotides in the rat. *Cell Mol Neurobiol*. 1994;14(5):475-486. doi:10.1007/BF02088832

20. Thorne RG, Nicholson C. In vivo diffusion analysis with quantum dots and dextrans predicts the width of brain extracellular space. *Proc Natl Acad Sci U S A*. 2006;103(14):5567-5572. doi:10.1073/pnas.0509425103

21. Abbott NJ. Evidence for bulk flow of brain interstitial fluid: Significance for physiology and pathology. *Neurochem Int*. 2004;45(4):545-552. doi:10.1016/j.neuint.2003.11.006

22. Sykova E, Nicholson C. Diffusion in Brain Extracellular Space. *Physiol Rev*. 2008;88:1277-1340. doi:10.1152/physrev.00027.2007.

23. Rosenberg GA, Kyner WT, Estrada E. Bulk flow of brain interstitial fluid under normal and hyperosmolar conditions. *Am J Physiol*. 1980;238(1):F42-F49. doi:10.1152/ajprenal.1980.238.1.f42

24. Fenstermacher JD, Patlak CS. The movements of water and solutes in brains of mammals. In: Pappius HM, Feindel W, eds. *Dynamics of Brain Edema*. Springer Nature; 1976:88-94.

25. Wolak DJ, Thorne RG. Diffusion of macromolecules in the brain: Implications for drug delivery. *Mol Pharm*. 2013;10(5):1492-1504. doi:10.1021/mp300495e

26. Thorne RG, Hrabetová S, Nicholson C. Diffusion of epidermal growth factor in rat brain extracellular space measured by integrative optical imaging. *J Neurophysiol*. 2004;92(6):3471-3481. doi:10.1152/jn.00352.2004

27. Nicholson C, Syková E. Extracellular space structure revealed by diffusion analysis. *Trends Neurosci*. 1998;21(5):207-215. doi:10.1016/S0166-2236(98)01261-2

28. Wolak DJ, Pizzo ME, Thorne RG. Probing the extracellular diffusion of antibodies in brain using in vivo integrative optical imaging and ex vivo fluorescence imaging. *J Control Release*. 2015;197:78-86. doi:10.1016/j.jconrel.2014.10.034

29. Deecke T. On the perivascular spaces in the nervous system. *J Insa*. 1874:322-330.

30. Hassin GB. Cerebrospinal Fluid: Its Origin, Nature and Function. *J Neuropathol Exp Neurol*. 1948;7:172-181.

31. Rennels ML, Gregory TF, Blaumanis OR, Fujimoto K, Grady PA. Evidence for a "Paravascular" fluid circulation in the mammalian central nervous system, provided by the rapid distribution of tracer protein throughout the brain from the subarachnoid space. *Brain Res*. 1985;326(1):47-63. doi:10.1016/0006-8993(85)91383-6

32. Zervas NT, Liszczak TM, Mayberg MR, Black PM. Cerebrospinal fluid may nourish cerebral vessels through pathways in the adventitia that may be analogous to systemic vasa vasorum. *J Neurosurg*. 1982;56(4):475-481. doi:10.3171/jns.1982.56.4.0475

33. Ichimura T, Fraser PA, Cserr HF. Distribution of extracellular tracers in perivascular spaces of the rat brain. *Brain Res*. 1991;545(1-2):103-113. doi:10.1016/0006-8993(91)91275-6

34. Foley CP, Nishimura N, Neeves KB, Schaffer CB, Olbricht WL. Real-time imaging of perivascular transport of nanoparticles during convection-enhanced delivery in the Rat cortex. *Ann Biomed Eng*. 2012;40(2):292-303. doi:10.1007/s10439-011-0440-0

35. Iliff JJ, Wang M, Liao Y, et al. A paravascular pathway facilitates CSF flow through the brain parenchyma and the clearance of interstitial solutes, including amyloid β. *Sci Transl Med*. 2012;4(147):147ra111-147ra111. doi:10.1126/scitranslmed.3003748

36. Pizzo ME, Wolak DJ, Kumar NN, et al. Intrathecal antibody distribution in the rat brain: surface diffusion, perivascular transport and osmotic enhancement of delivery. *J Physiol*. 2018;596(3):445-475. doi:10.1113/JP275105

37. Hannocks MJ, Pizzo ME, Huppert J, et al. Molecular characterization of perivascular drainage pathways in the murine brain. *J Cereb Blood Flow Metab*. 2018;38(4):669-686. doi:10.1177/0271678X17749689

38. Davson H, Segal MB. *Physiology of the CSF and Blood-Brain Barriers*. Boca Raton: CRC Press; 1996.

39. Yang L, Kress BT, Weber HJ, et al. Evaluating glymphatic pathway function utilizing clinically relevant intrathecal infusion of CSF tracer. *J Transl Med*. 2013;11(1):107. doi:10.1186/1479-5876-11-107

40. Nicholson C, Tao L. Hindered diffusion of high molecular weight compounds in brain extracellular microenvironment measured with integrative optical imaging. *Biophys J*. 1993;65(6):2277-2290. doi:10.1016/S0006-3495(93)81324-9

41. Schindelin J, Arganda-Carreras I, Frise E, et al. Fiji: an open-source platform for biological-image analysis. *Nat Methods*. 2012;9(7):676-682. doi:10.1038/nmeth.2019

42. Watson C, Paxinos G. *The Rat Brain in Stereotaxic Coordinates*. 6th ed. Amsterdam: Elsevier; 2007.

43. Szentistvanyi I, Patlak CS, Ellis RA, Cserr HF. Drainage of interstitial fluids from different regions of the rat brain. *Ren Physiol*. 1984;246(6):835-844.

44. Roth E, Glick Azaria A, Girshevitz O, Bitler A, Garini Y. Measuring the Conformation and Persistence Length of Single-Stranded DNA Using a DNA Origami Structure. *Nano Lett*. 2018;18(11):6703-6709. doi:10.1021/acs.nanolett.8b02093

45. Goddard NL, Bonnet G, Krichevsky O, Libchaber A. Sequence dependent rigidity of single stranded DNA. *Phys Rev Lett*. 2000;85(11):2400-2403. doi:10.1103/PhysRevLett.85.2400

46. Plumridge A, Meisburger SP, Andresen K, Pollack L. The impact of base stacking on the conformations and electrostatics of single-stranded DNA. *Nucleic Acids Res*. 2017;45(7):3932-3943. doi:10.1093/nar/gkx140

47. McIntosh DB, Duggan G, Gouil Q, Saleh OA. Sequence-dependent elasticity and electrostatics of single-stranded DNA: Signatures of base-stacking. *Biophys J*. 2014;106(3):659-666. doi:10.1016/j.bpj.2013.12.018

48. Bosco A, Camunas-Soler J, Ritort F. Elastic properties and secondary structure formation of single-stranded DNA at monovalent and divalent salt conditions. *Nucleic Acids Res*. 2014;42(3):2064-2074. doi:10.1093/nar/gkt1089

49. Novak U, Kaye AH. Extracellular matrix and the brain: Components and function. *J Clin Neurosci*. 2000;7(4):280-290. doi:10.1054/jocn.1999.0212

50. Ghosh MK, Ghosh K, Cohen JS. Phosphorothioate-phosphodiester oligonucleotide co-polymers: assessment for antisense application. *Anticancer Drug Des*. 1993;8(1):15-32. http://www.ncbi.nlm.nih.gov/pubmed/8386513.

51. Brown DA, Kang SH, Gryaznov SM, et al. Effect of phosphorothioate modification of oligodeoxynucleotides on specific protein binding. *J Biol Chem*. 1994;269(43):26801-26805.

52. Srinivasan SK, Tewary HK, Iversen PL. Characterization of Binding Sites, Extent of Binding, and Drug Interactions of Oligonucleotides with Albumin. *Antisense Res Dev*. 1995;5(2):131-139. doi:10.1089/ard.1995.5.131

53. Geary RS, Watanabe TA, Truong L, et al. Pharmacokinetic properties of 2'-O-(2-methoxyethyl)-modified oligonucleotide analogs in rats. *J Pharmacol Exp Ther*. 2000;296(3):890-897. http://www.ncbi.nlm.nih.gov/pubmed/11181921.

54. Tibbling G, Link H, Öhman S. Principles of albumin and igg analyses in neurological disorders. I. Establishment of reference values. *Scand J Clin Lab Invest*. 1977;37(5):385-390. doi:10.1080/00365517709091496

55. Link H, Tibbling G. Principles of albumin and igg analyses in neurological disorders. II. Relation of the concentration of the proteins in serum and cerebrospinal fluid. *Scand J Clin Lab Invest*. 1977;37(5):391-396. doi:10.1080/00365517709091497

56. Jesse S, Brettschneider J, Süssmuth SD, et al. Summary of cerebrospinal fluid routine parameters in neurodegenerative diseases. *J Neurol*. 2011;258(6):1034-1041. doi:10.1007/s00415-010-5876-x

57. Brightman MW, Reese TS. Junctions Between Intimately Apposed Cell Membranes in the Vertebrate Brain. *J Cell Biol*. 1969;40(3):648-677. doi:10.1083/jcb.40.3.648

58. Fossan G, Cavanagh ME, Evans CAN, et al. CSF-Brain permeability in the immature sheep fetus: A CSF-brain barrier. *Dev Brain Res*. 1985;18(1-2):113-124.

doi:10.1016/0165-3806(85)90255-X

59. Saunders NR, Dziegielewska KM, Møllgård K, Habgood MD. Physiology and molecular biology of barrier mechanisms in the fetal and neonatal brain. *J Physiol*. 2018;596(23):5723-5756. doi:10.1113/JP275376

60. Aspelund A, Antila S, Proulx ST, et al. A dural lymphatic vascular system that drains brain interstitial fluid and macromolecules. *J Exp Med*. 2015;212(7):991-999. doi:10.1084/jem.20142290

61. Louveau A, Smirnov I, Keyes TJ, et al. Structural and functional features of central nervous system lymphatic vessels. *Nature*. 2015;523(7560):337-341. doi:10.1038/nature14432

62. Faber WM. The nasal mucosa and the subarachnoid space. *Am J Anat*. 1937;62(1):121-148. doi:10.1002/aja.1000620106

63. Kida S, Pantazis A, Weller RO. CSF drains directly from the subarachnoid space into nasal lymphatics in the rat. Anatomy, histology and immunological significance. *Neuropathol Appl Neurobiol*. 1993;19(6):480-488. doi:10.1111/j.1365-2990.1993.tb00476.x

64. Bradbury MW, Westrop RJ. Factors influencing exit of substances from cerebrospinal fluid into deep cervical lymph of the rabbit. *J Physiol*. 1983;339(1):519-534. doi:10.1113/jphysiol.1983.sp014731

65. Koh L, Zakharov A, Johnston M. Integration of the subarachnoid space and lymphatics: Is it time to embrace a new concept of cerebrospinal fluid absorption? *Cerebrospinal Fluid Res*. 2005;2:33-38. doi:10.1186/1743-8454-2-6

66. Wurster CD, Winter B, Wollinsky K, et al. Intrathecal administration of nusinersen in adolescent and adult SMA type 2 and 3 patients. *J Neurol*. 2019;266(1):183-194. doi:10.1007/s00415-018-9124-0

67. Mousa MA, Aria DJ, Schaefer CM, et al. A comprehensive institutional overview of intrathecal nusinersen injections for spinal muscular atrophy. *Pediatr Radiol*. 2018;48(12):1797-1805. doi:10.1007/s00247-018-4206-9

68. Meyer K, Ferraiuolo L, Schmelzer L, et al. Improving single injection CSF delivery of AAV9-mediated gene therapy for SMA: A dose-response study in mice and nonhuman primates. *Mol Ther*. 2015;23(3):477-487. doi:10.1038/mt.2014.210

69. Castle MJ, Cheng Y, Asokan A, Tuszynski MH. Physical positioning markedly enhances brain transduction after intrathecal AAV9 infusion. *Sci Adv*. 2018;4(11):eaau9859. doi:10.1126/sciadv.aau9859

70. Xie L, Kang H, Xu Q, et al. Sleep Drives Metabolite Clearance from the Adult Brain. *Science (80-)*. 2013;342(6156):373-377. doi:10.1126/science.1241224

71. Ma Q, Ries M, Decker Y, et al. Rapid lymphatic efflux limits cerebrospinal fluid flow to the brain. *Acta Neuropathol*. 2018;137(1):151-165. doi:10.1007/s00401-018-1916-x

72. Gakuba C, Gaberel T, Goursaud S, et al. General Anesthesia Inhibits the Activity of the " Glymphatic System ." *Theranostics*. 2018;8(3). doi:10.7150/thno.19154

73. Abbott NJ, Pizzo ME, Preston JE, Janigro D, Thorne RG. The role of brain barriers in fluid movement in the CNS: is there a 'glymphatic' system? *Acta Neuropathol*. 2018;135(3):387-407. doi:10.1007/s00401-018-1812-4

74. Rigo F, Chun SJ, Norris DA, et al. Pharmacology of a Central Nervous System Delivered 2'-O-Methoxyethyl-Modified Survival of Motor Neuron Splicing Oligonucleotide in Mice and Nonhuman Primates. *J Pharmacol Exp Ther*. 2014;350(1):46-55. doi:10.1124/jpet.113.212407

75. Finkel RS, Mercuri E, Darras BT, et al. Nusinersen versus Sham Control in Infantile-Onset Spinal Muscular Atrophy. *N Engl J Med*. 2017;377(18):1723-1732. doi:10.1056/NEJMoa1702752

76. Tabrizi SJ, Leavitt BR, Landwehrmeyer GB, et al. Targeting Huntingtin Expression in Patients with Huntington's Disease. *N Engl J Med*. 2019:NEJMoa1900907. doi:10.1056/NEJMoa1900907

77. Miller TM, Pestronk A, David W, et al. An antisense oligonucleotide against SOD1 delivered intrathecally for patients with SOD1 familial amyotrophic lateral sclerosis: A phase 1, randomised, first-in-man study. *Lancet Neurol*. 2013;12(5):435-442. doi:10.1016/S1474-4422(13)70061-9

78. Li D, Liu C, Yang C, et al. Slow intrathecal injection of rAAVrh10 enhances its transduction of spinal cord and therapeutic efficacy in a mutant SOD1 model of ALS. *Neuroscience*. 2017;365:192-205. doi:10.1016/j.neuroscience.2017.10.001

79. Tangen K, Mehta AI, Linninger AA. Cerebrospinal Fluid Dynamics and Intrathecal Delivery. In: Krames E, Peckham PH, Rezai A, eds. *Neuromodulation*. 2nd ed. Elsevier Ltd; 2018:829-846. doi:10.1016/B978-0-12-805353-9.00067-X

80. Calias P, Banks WA, Begley D, Scarpa M, Dickson P. Intrathecal delivery of protein therapeutics to the brain: A critical reassessment. *Pharmacol Ther*. 2014;144(2):114-122. doi:10.1016/j.pharmthera.2014.05.009

81. *FDA Approves First Treatment for a Form of Batten Disease*.; 2017. https://www.fda.gov/news-events/press-announcements/fda-approves-first-treatment-form-batten-disease.

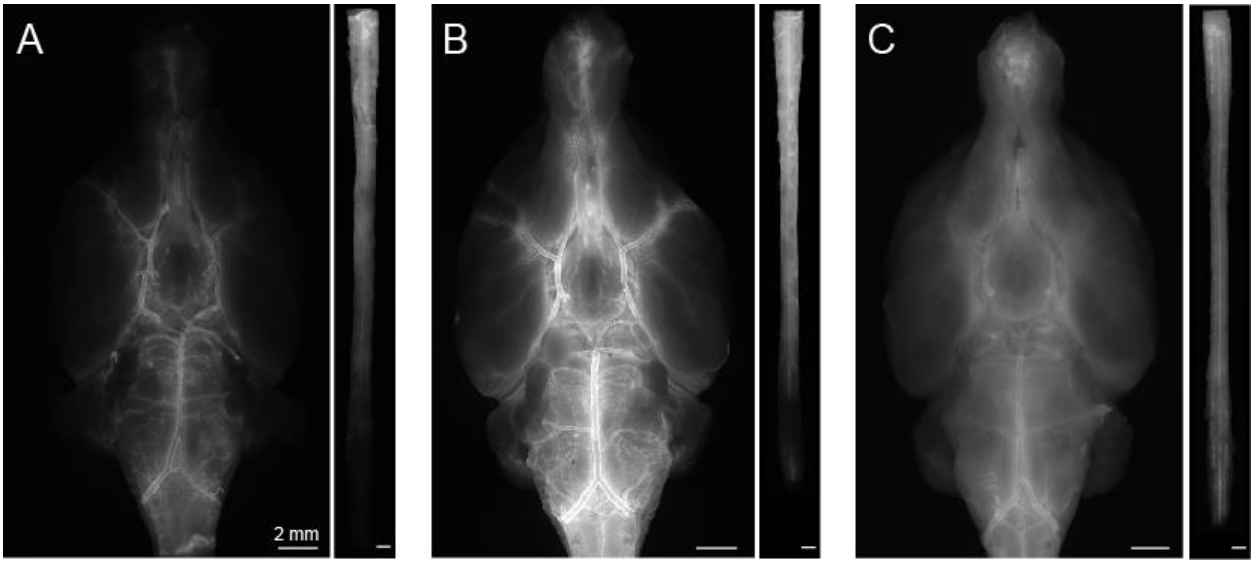

Figure 1: *Ex vivo* fluorescenence imaging of the ventral surface of the brain and spinal cord for rats receiving an intrathecal infusion of A) PS-ASO B) PS-ASO with hyperosmolar mannitol, and C) 2'MOE-ASO. Fluorescent ASO signal can be seen in the perivascular spaces of the large blood vessels on the ventral brain surface.

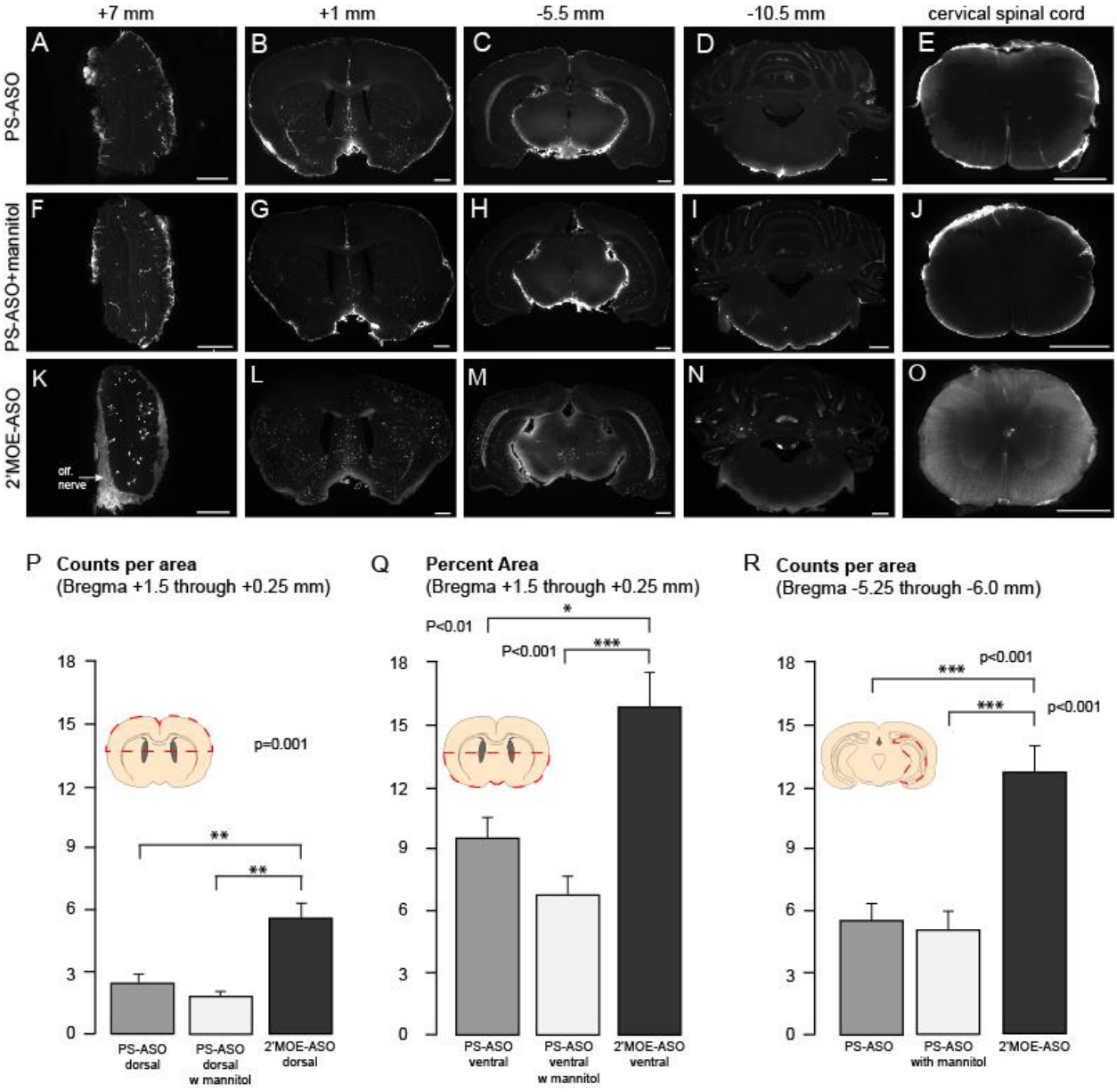

Figure 2: *Ex vivo* fluorescence imaging of representative coronal sections from rostral to caudal after intrathecal infusion of (A-E) PS-ASO, (F-J) PS-ASO with hyperosmolar mannitol, and (K-O) 2'MOE-ASO. Coronal sections demonstrated a diffuse surface gradient visible at the ventral surface that was more prominent for the 2'MOE-ASO. Punctate signal in the coronal sections also revealed perivascular transport of the ASOs. Fluorescent puncta were more sparse for the sections corresponding to PS-ASO and PS-ASO with mannitol, particularly in the dorsal halves

of the section and in subcortical structures including the striatum (B,G,L). (P) Quantification of fluorescent ASO signal in the dorsal half (fluorescent counts in the outlined tissue area per square millimeter) using 8 tissue sections per animal (*N*= 7 animals) centered 1 mm anterior to bregma demonstrated that 2'MOE-ASO access to the perivascular space is significantly greater compared with PS-ASO and PS-ASO with mannitol (One-way ANOVA on ranks, post-hoc Tukey Test). (Q) Quantification of fluorescent ASO signal (percent of the outlined tissue area containing fluorescent signal) using 8 tissue sections per animal (*N*=7 animals) in the ventral half of tissue sections centered 1 mm anterior to bregma demonstrated that the 2'MOE-ASO distributes to a greater extent than PS-ASO or PS-ASO with mannitol through a combination of diffusion at the ventral surface and perivascular access (One-way ANOVA, post-hoc Holm-Sidak test). (R) Quantification of fluorescent ASO signal in the outlined area (fluorescent counts per square millimeter) using 8 tissue sections per animal (*N*=7 animals) centered at 5.5 mm posterior to bregma demonstrated that 2'MOE-ASO access to the perivascular space is greater compared with PS-ASO and PS-ASO with mannitol (One-way ANOVA, post-hoc Holm-Sidak).

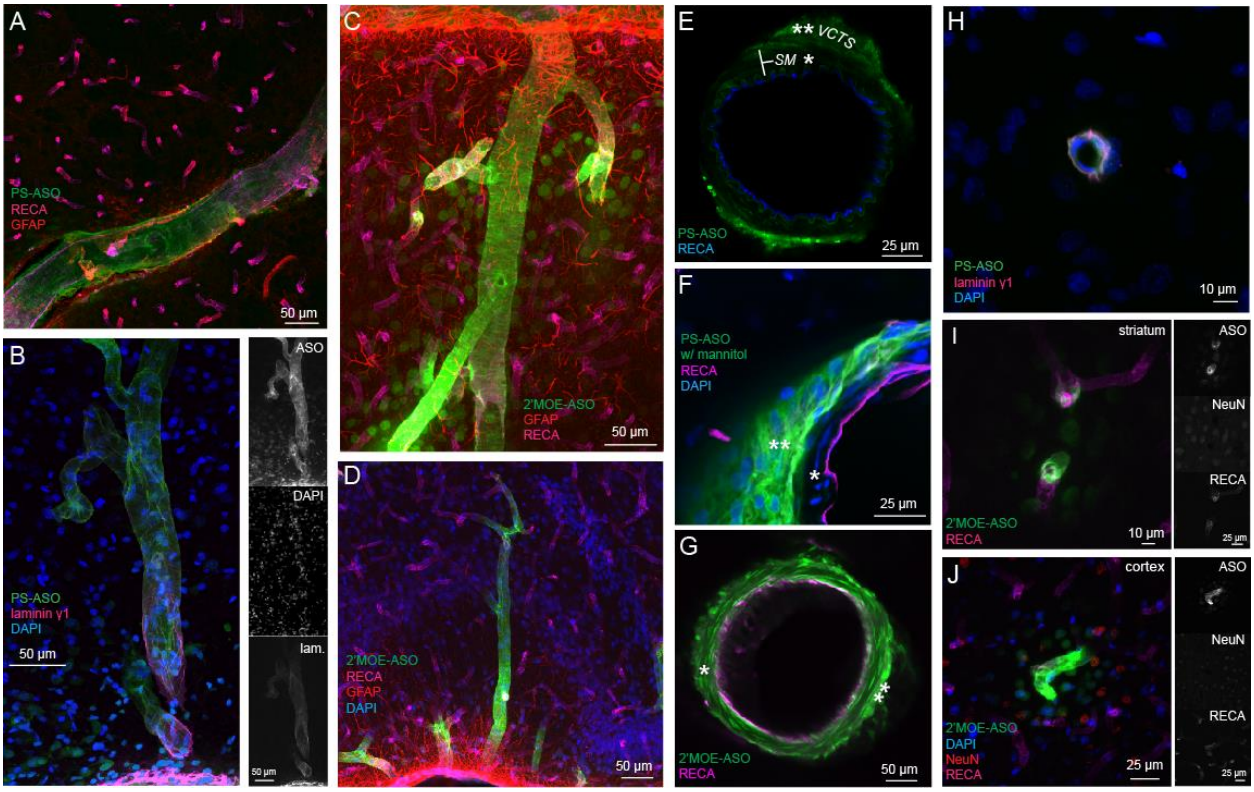

Figure 3: Confocal microscopy demonstrates ASO distribution to the perivascular spaces associated with vessels of all caliber. PS-ASO is found surrounding penetrating arterioles (A) and putative venules (B). 2'MOE-ASO was similarly found along the perivascular spaces of arterioles (C) and putative venules (D). Selective entry into the basement membrane of the smooth muscle layer (*) was observed in large caliber arteries. PS-ASO alone (E) and PS-ASO co-infused with hyperosmolar mannitol (F) demonstrated restricted acceess to the smooth muscle, with ASO signal largely localized in the vascular connective tissue space (**). 2'MOE-ASO signal distributed through the smooth muscle layer as well as the connective tissue space (G). Both PS-ASO (H) and 2'MOE-ASO (I) appeared to distribute to the perivascular space at the microvessel level. ASO signal can be found within neurons and non-neuronal cells within

close proximity to vessels with perivascular signal as demonstrated by colocalization of ASO with NeuN and/or DAPI (I,J), as well as within cells near the CSF-brain interface (B).

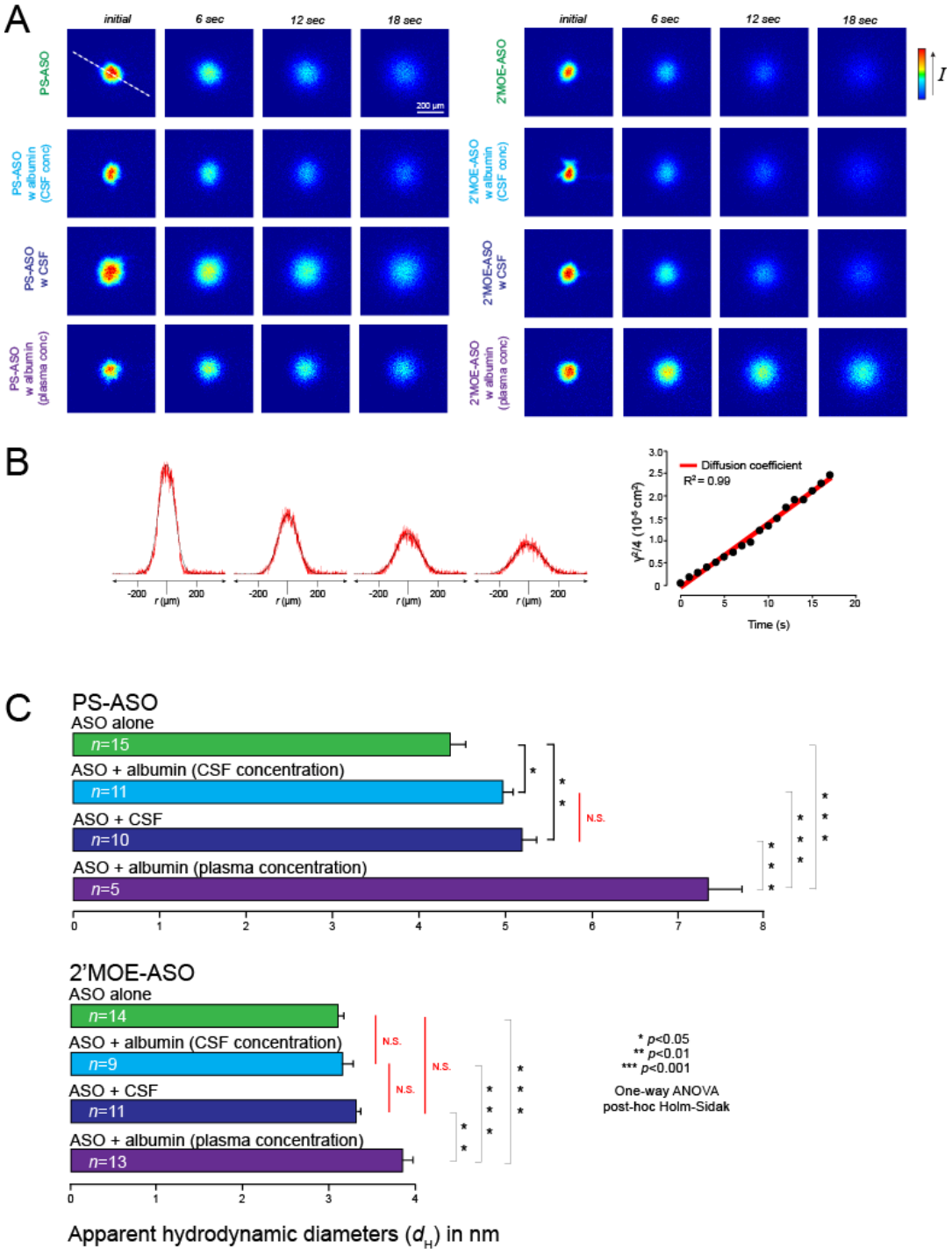

Figure 4: Using integrative optical imaging, diffusion coefficients and apparent hydrodynamic diameters were found for fluorescently-labeled PS-ASO and 2'MOE-ASO by themselves or co-

injected with albumin at CSF concentration, rat CSF, and albumin at plasma concentration. (A) Representative diffusion cloud images taken at 6 second intervals corresponding to injection of each ASO in dilute agarose. Dashed line denotes axis from which the representative fluorescence intensity curve and diffusion coefficient were extracted (B). Analysis of apparent hydrodynamic diameters for each ASO (C) demonstrated that the PS-ASO binds to albumin at CSF concentration, CSF, and albumin at plasma concentration such that there was a significant increase in the apparent hydrodynamic diameter of the PS-ASO. Binding only caused an increase in apparent hydrodynamic diameter for the 2'MOE-ASO when albumin was present at plasma concentration (One-way ANOVA, post-hoc Holm-Sidak). The apparent hydrodynamic diameter of the PS-ASO was significantly larger than that of the 2'MOE-ASO ($p<0.0001$, values found in text).

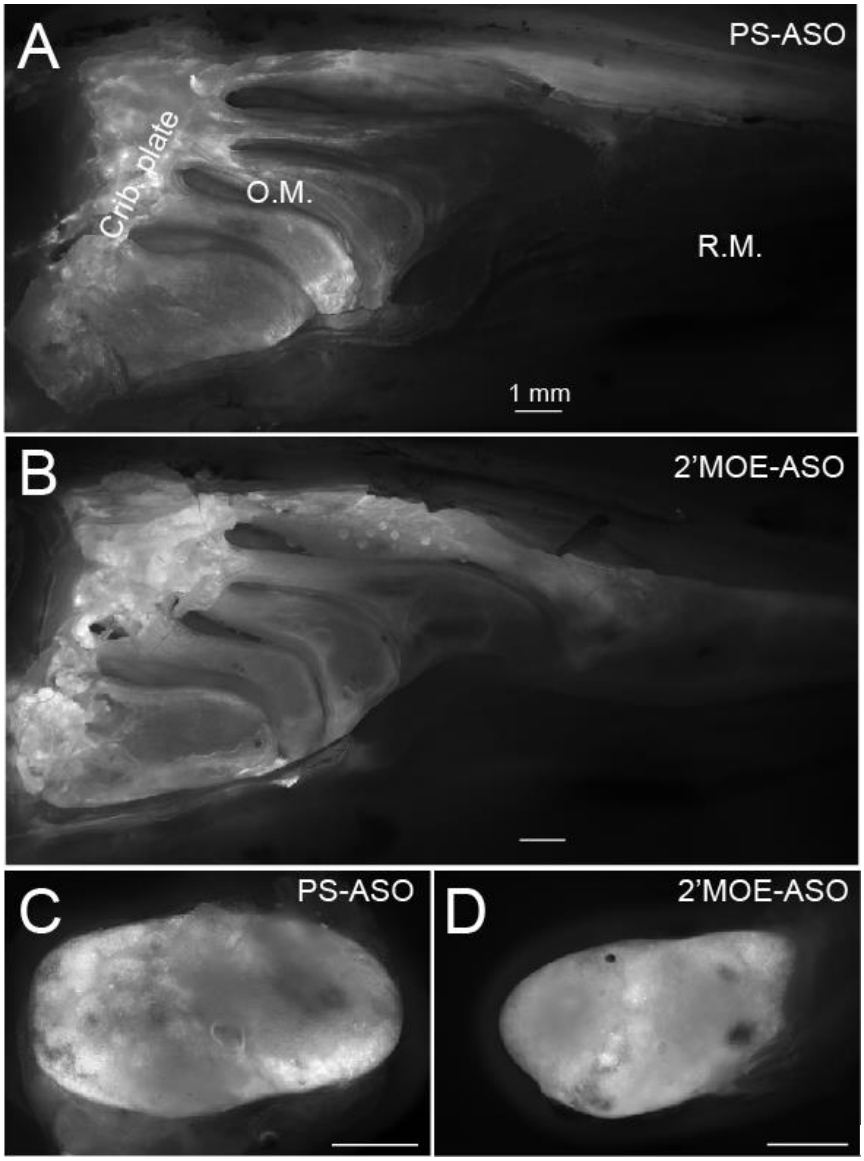

Figure 5: ASO drainage via an olfactory pathway following intrathecal administration. *Ex vivo* fluorescence imaging showed PS-ASO (A) and 2'MOE-ASO (B) in the nasal passages, particularly the cribriform plate and the olfactory mucosa (O.M.). Signal was not seen in the respiratory mucosa (R.M.). The deep cervical lymph nodes consistently displayed fluorescent signal following PS-ASO (C) and 2'MOE-ASO (D) infusion.

CHAPTER 4
CNS distribution and transport mechanisms following intrathecal delivery of phosphorodiamidate morpholino oligonucleotides

Brynna Wilken-Resman[1], Charles Lauhon[1], and Robert G. Thorne[1,2]
[1]School of Pharmacy, Division of Pharmaceutical Sciences; University of Wisconsin-Madison, Madison, Wisconsin, USA [2]Denali Therapeutics, San Francisco, California, USA

Abstract

Phosphorodiamidate morpholino oligonucleotides (PMOs) are antisense oligonucleotide (ASO) analogs designed to be uncharged and inhibit protein translation independently of RNase H. Unlike single stranded DNA and many other types of ASOs, PMOs possess a neutral backbone and exhibit low protein binding. Here, we examined the biodistribution of fluorophore-conjugated PMO in the rat central nervous system following intrathecal administration at the cisterna magna. We hypothesized that the uncharged nature of PMOs might result in pronounced differences in their CSF-to-brain biodistribution as compared with charged ASOs. However, PMO tracers were found to distribute along the perivascular spaces of arterioles, venules, and microvessels and also demonstrate a diffusive gradient at the CSF-facing pial surface similar to other previously studied ASOs with charged backbones (e.g. 2'MOE-ASO). Our studies also demonstrated an olfactory clearance route was utilized for PMO drainage to peripheral lymphatics, as with other charged ASOs. This study of PMO distribution from CSF-to-brain represents, to our knowledge, the first such detailed examination for an uncharged nucleic acid analog and hints at further complexity in the factors governing oligonucleotide delivery to the CNS following intrathecal administration.

Introduction

Within the last four years, three antisense oligonucleotide (ASO) therapeutics have received FDA approval, with many more in clinical trials.[1,2] These ASOs, nusinersen, eteplirsen, and inotersen share the same general structure as they are single stranded oligonucleotides ranging from 18-30 bases[3–5], yet they contain different chemical modifications to the typical phosphodiester backbone and deoxyribose or ribose sugar found in unmodified DNA or RNA in

addition to having different sequences to allow for base pairing to target RNA. Approval of nusinersen in 2016 for the treatment of spinal muscular atrophy marked the first approval for an ASO targeting the central nervous system (CNS). [4] Nusinersen is administered as an intrathecal injection directly into the cerebrospinal fluid (CSF) since intravenous administration of ASOs has been shown to result in negligible brain exposure[6,7] because their size and charge prevent them from crossing the blood-brain barrier. [8] Intrathecal administration effectively bypasses the blood-brain barrier by depositing the ASO into the CSF of the subarachnoid space surrounding the brain and spinal cord. Sufficient ASO distribution to target sites in the brain and spinal cord therefore depends on the transport mechanisms that govern macromolecule distribution from the CSF to CNS tissues. The two mechanisms that are thought to govern macromolecule biodistribution in the central compartment are diffusion from CSF-facing brain and spinal cord surfaces and convection and/or dispersion through perivascular spaces, a compartment containing fluid and connective tissue surrounding cerebral blood vessels. [9–11] Diffusion, or the random movement of solute particles driven by a concentration gradient, is considered the dominant transport mechanism in the narrow (~40-60 nm) extracellular spaces[12], as it is thought that the high hydraulic resistance of these narrow channels prevents any appreciable bulk flow. [13] Diffusion of macromolecules through the extracellular space can be hindered by cellular and extracellular obstacles, including the presence of negatively charged proteoglycans in the extracellular matrix. [10,14] While diffusion is likely an inefficient process for macromolecules over long distances such as would be required for whole brain distribution,[10,15] evidence suggests that bulk flow or convection may occur in perivascular spaces (PVS). [16–19] Tracer distribution studies have demonstrated that intrathecal infusion can result in rapid perivascular signal surrounding blood vessels of all type and caliber in cortical and subcortical brain regions. [9,20]

An interesting recent finding regarding ASO distribution via these two transport mechanisms is that ASOs differing in sequence and chemical modification have dramatically different CNS distributions following intrathecal administration (Wilken-Resman and Thorne, unpublished, Chapter 3) and that this may be a result of the sequence and chemistry specific to each ASO impacting hydrodynamic size, electrostatic interactions, and/or capacity for binding. These factors could affect how an ASO interacts with the unique anatomy and physiology associated with diffusion in the extracellular spaces and distribution along perivascular spaces. One type of ASO, the phosphorodiamidate morpholino oligonucleotide (PMO), differs from the standard single stranded DNA chemistry in that it substitutes a neutral phosphorodiamidate internucleoside linkage for a negatively charged phosphodiester or phosphorothioate linkage and replaces the typical five-carbon ribose ring with a six-carbon morpholine ring.[21] In addition to lacking a negative charge, these PMOs exhibit low binding to plasma proteins. [22] These differences in charge and binding make PMOs an intriguing ASO to examine for CNS distribution after intrathecal administration. While there is an FDA approved PMO, eteplirsen, for the treatment of Duchenne muscular dystrophy[1], it is administered intravenously to target dystrophin pre-mRNA in the periphery.[3] There is currently no PMO antisense oligonucleotide approved for intrathecal administration to treat a disorder of the CNS and there is a gap in the literature regarding CNS delivery and distribution of ASOs with PMO modifications. The present study aims to explicitly address this gap by examining how a labeled PMO antisense oligonucleotide distributes to CNS tissue following intrathecal administration in rats.

Materials and methods

Ethical approval

Experiments were conducted at the University of Wisconsin-Madison in compliance with the National Institutes of Health Guide for the Care and Use of Laboratory Animals and approved by the local Institutional Animal Care and Use Committee. Animals were housed in a climate-controlled room and kept on a 12:12 h light/dark cycle. Animals had access to food and water *ad libitum*. Experiments were terminal and all efforts were made to minimize animal pain and distress.

Cisternal intrathecal infusion in rats

Sprague-Dawley rats (female; 180-270 g; ~10-20 weeks of age; Envigo, Indianapolis, IN, USA) were anesthetized with an initial dose of urethane (1.2 g kg^{-1} I.P.) and supplemented as needed (0.375 g kg^{-1}) to reach a surgical plane of anesthesia, as demonstrated by the absence of pedal or palpebral reflexes. Body temperature was kept at 37 °C using a homeothermic blanket system (Harvard Apparatus, Holliston, MA, USA). Atropine sulfate (0.1 mg/kg S.C. every 2 h) was administered to reduce bronchial secretions. Rats were tracheotomized and an analgesic (2 % lidocaine hydrochloride, 0.05 mL S.C.) was administered at the scalp. Rats were placed prone in a stereotaxic frame (Stoelting Co., Wood Dale, IL, USA) with the head approximately horizontal. Intrathecal infusion at the cisterna magna was performed as detailed previously. An incision was made along the midline of the scalp and dorsal neck and the underlying muscles were retracted to expose the atlanto-occipital membrane. This membrane was carefully removed, revealing the dura mater covering the cisterna magna. A small hole was carefully punctured in the dura with a 30-G dental needle and a custom cannula was inserted and advanced 1 mm into

the cisterna magna. The cannula consisted of 1.5 cm 33-G polyetheretherketone (PEEK; Plastics One Inc., Roanoke, VA, USA) connected to tubing (PE-10; Solomon Scientific, San Antonio, TX, USA) leading to a Hamilton Syringe controlled by an infusion pump. Cyanoacrylate was used to fix the cannula in position with the dura sealed around it. Tubing and syringe were filled with infusate (80 µL fluorescently labeled PMO) prior to cannula insertion. The 50 min infusion commenced. The infusion rate of 1.6 µL/min was chosen because it is approximately half the cerebrospinal fluid production rate in the rat[23] and has been shown to not significantly increase intracranial pressure. [24] Following intrathecal infusion, the rat was placed supine and the abdominal aorta was cannulated. The animal was euthanized 30 min post-infusion by exsanguination via abdominal aorta perfusion with 50 mL ice-cold 0.01 M PBS (pH 7.4) at a rate of 15 mL min^{-1}, followed by perfusion with 4% paraformaldehyde (PFA) in 0.1 M phosphate buffer. $N = 5$ rats.

Antisense oligonucleotide purchase and preparation

The phosphorodiamidate morpholino oligonucleotide (PMO) used in the present study was purchased from Gene Tools (Philomath, OR, USA). Carboxyfluorescein was covalently attached at a 1:1 ratio on the 5' end of the oligonucleotide and added relatively little (< 6 %) to the overall molecular weight of the ASO. The PMO was received as a lyophilized powder, reconstituted with 0.01 M PBS to a concentration of 150 µM, and stored in the dark at room temperature, as per manufacturer guidelines, until the time of use. The nucleotide sequence for the PMO is as follows, from 5' to 3': CTCAGTAACATTGACACCAC and the molecular weight was 6.7 kDa.

Ex vivo *fluorescence imaging and image processing*

Brain, spinal cord, superficial and deep cervical lymph nodes, and nasal passages were removed and immediately imaged using an MVX10 Macroview microscope (Olympus, Tokyo, Japan) coupled with an X-Cite-120Q illuminator (Lumen Dynamics Group, Inc., Mississauga, Ontario, Canada), an Orca-flash 2.8 CMOS camera (Hamamatsu, Hamamatsu City, Japan) and using a FITC filter (Chroma, U-M49002XL, Bellows Falls, VT, USA). The dorsal and ventral brain surfaces, spinal cord, and nasal passages were each imaged in multiple overlapping sections. When necessary, planes of focus were autoblended and overlapping sections were aligned manually using Photoshop (Adobe Systems, San Jose, CA, USA) to create a single image. The brain and anterior cervical spinal cord were kept at 4 °C overnight, then were sectioned coronally (100 µm) using a vibratome (VT1000S; Leica Microsystems, Wetzlar, Germany) and immediately imaged on a wet petri dish for detection of the fluorescently labeled PMO.

Immunohistochemistry and confocal imaging

Free-floating coronal sections were placed in blocking buffer consisting of 5% goat or donkey serum or 2.5 % goat and 2.5 % donkey serum in 0.01 M PBS with 0.03 % Triton-X for 1 h at room temperature, then incubated with primary antibody in blocking buffer overnight at 4°C. Primary antibodies and their dilutions include rat endothelial cell antigen-1 (RECA-1; ab9774; Abcam, Cambridge, MA, USA; dilution 1:1000), rabbit-anti-NeuN (ab177487; Abcam, Cambridge, MA, USA; dilution 1:500), and chicken-anti-GFAP (NBP1-05196; Novus Biologicals, Littleton, OH, USA; dilution 1:1000). After primary incubation, sections were washed with ice cold PBS 3 times for 15 min each and incubated in secondary antibody solution in blocking buffer at a dilution of 1:500 for 2 h at room temperature. Secondary antibodies used

include goat-anti-mouse 647 (ab150119; Abcam), goat anti-rabbit 594 (A11012; Life Technologies, Eugene, OR, USA), and goat-anti-chicken 594 (ab150172; Abcam). Sections were then washed with PBS and incubated with DAPI (Life Technologies; 2 μg mL^{-1}) for 20 min at room temperature and washed 3 more times in PBS before being mounted on slides using Prolong Diamond Antifade (Life Technologies). Images were acquired using an A1R confocal microscope with NIS Elements (Nikon, Tokyo, Japan).

Diffusion measurements in free medium using integrative optical imaging

The diffusion coefficient (D) of the PMO in free media its associated apparent hydrodynamic diameter (d_H) were found using the integrated optical imaging (IOI) technique. [12,15,25,26] This technique involves pressure ejection of the fluorescently labeled PMO from a glass micropipette (tip diameter 5-10 μm, catalog 617000, A-M Systems, Carlsborg, WA, USA) into a medium of 0.3 % NuSieve GTG agarose (FMC, Philadelphia, PA, USA) in 154 mM NaCl, maintained at 37.0 ± 0.5 °C. PMO ejection volume was approximately 25-50 pL, resulting from a 100 millisecond pulse of nitrogen (Toohey Spritzer, Toohey, Fairfield, NJ, USA), approximating a point source. The resulting diffusion clouds were imaged at 1 s intervals using a custom[25] MATLAB program (MathWorks) and epifluorescence microscopy. The system consisted of an Olympus BX61WI microscope equipped with a water-immersion objective (UM PlanFl 10x, NA 0.3; Olympus, Center Valley, PA, USA), (FITC) filter set (Chroma, Bellows Falls, VT, USA), and a CCD camera (Cool-Snap HQ^2; Photometrics, Tucson, AZ, USA). The following equations describe how the 3D diffusion clouds are mapped onto the camera according to diffusion theory[25,26]:

$$I_i(r, \gamma_i) = E_i \exp\left[-(r/\gamma_i)^2\right] \qquad \text{Equation 1}$$

and

$$\gamma_i{}^2 = 4D(t_i + t_0) \qquad \text{Equation 2}$$

where I_i represents the fluorescence intensity of the ith image at a distance, r, from the injection point and E_i represents the defocused point spread of the microscope objective. Fluorescence intensity data was extracted from the diffusion images along six axes. Equation 1 was fit to the upper 90 % of the resulting intensity curves using a nonlinear simplex algorithm in a separate custom MATLAB program. Fits returned estimates for a parameter, γ_i, at a time interval (t_i) after injection approximating a point source (t_0). Linear regression of $\gamma^2/4$ vs t_i yielded the slope, which is equivalent to the free diffusion coefficient D based on Equation 2. The highest and lowest of the D values obtained along the six axes were discarded and the average D was calculated from the four remaining axes. The apparent hydrodynamic diameter (d_H) was then calculated from the Stokes-Einstein equation using the average D value:

$$d_H = (kT)/(3\pi\eta D) \qquad \text{Equation 3}$$

where k is Boltzmann's constant, T is absolute temperature, and η is the viscosity of water (6.9152×10^{-4} Pa s at T = 310 K).

Results

Apparent hydrodynamic size

We first characterized the free diffusion of a carboxyfluorescein-labeled PMO using the method of integrative optical imaging[12,25,26] in order to obtain its hydrodynamic size in solution at 37°C. Injection of fluorescently labeled PMO in dilute agarose and fitting the resulting profiles with diffusion theory yielded a free diffusion coefficient (D) of (2.09 ± 0.05) x 10^{-6} cm^2s^{-1} (n =15). Using D and the Stokes-Einstein equation the apparent hydrodynamic diameter (d_H) of the PMO was calculated to be 3.15 ± 0.07 nm.

Whole brain ex vivo *fluorescence imaging*

We next studied the biodistribution of this PMO-carboxyfluorescein conjugate following intracisternal infusion in urethane-anesthetized adult Sprague-Dawley rats, using a paradigm identical to that previously published[9] and used for earlier studies examining the CNS distribution of ASOs with charged backbones (Wilken-Resman and Thorne, unpublished, Chapter 3). The PMO distributed within perivascular spaces along the large blood vessels on the ventral brain surface (Figure 1A), including the Circle of Willis (CoW) (Figure 1D), and the dorsal brain surface (Figure 1B), including the middle cerebral artery (MCA) (Figure 1C). Surface signal appeared diffuse, likely due to diffusion from the pial surface as well as diffusion from the perivascular spaces. Punctate signal was also visualized on the brain surface, consistent with fluorescence surrounding penetrating blood vessels entering the brain perpendicular to the brain surface (Figure 1D).

Fluorescent signal associated with perivascular spaces surrounding vessels of differing type and caliber

Confocal microscopy was used to visualize the location of PMO within the PVS of both arterioles (Figure 2A) and venules (Figure 2B) in coronal sections. A cross-sectional view of the internal carotid artery (Figure 2C) demonstrated that the PMO conjugate distributed to the vascular connective tissue space of the tunica adventitia and the basement membrane associated with the smooth muscle cells in the tunica media of large arteries. PMO signal was also found surrounding vessels of all caliber down to the microvessel level (Figure 2D). Punctate PMO signal was occasionally visualized colocalizing with the neuronal marker NeuN (Figure 2E).

Ex vivo *fluorescence imaging of coronal brain sections*

Lower resolution imaging of coronal tissue sections (100 µm) were imaged to visualize the surface diffusion gradient and perivascular distribution of the fluorescently labeled PMO, as described previously (Pizzo et al. 2018). The most notable and consistent aspect of PMO biodistribution in these sections was a diffuse gradient evident primarily at the ventral brain surface. Perivascular PMO signal was also consistently apparent in the cortex as well as certain subcortical structures, e.g. the caudoputamen (Figure 3B) and posterior hippocampus (Figure 3C); PMO signal was less apparent or variably present in other subcortical structures such as the anterior hippocampus and the thalamus (Figure 3D). Perivascular PMO signal was rarely found in the brainstem, but punctate perivascular signal was frequently found in the cerebellar nuclei (Figure 3E). PMO signal in the cervical spinal cord sections was diffuse (Figure 3F). There was a general trend throughout the neuroaxis for greater perivascular access in the ventral half of the brain compared to the dorsal half.

Olfactory drainage pathway

Drainage of PMO from the CSF appeared to occur at least in part via an olfactory pathway. Prominent fluorescent signal consistently appeared in the olfactory nerve layer surrounding the olfactory bulb (Figure 4A) as well as in the cribriform plate and the olfactory mucosa of the nasal passages (Figure 4B and 4C). The deep cervical lymph nodes in the neck were also found to consistently contain signal demonstrating PMO drainage to peripheral lymphatics (Figure 4D).

PMO interactions with albumin

As protein binding to CSF proteins has been suggested to play a role in impacting ASO biodistribution in brain following CSF infusions (Wilken-Resman and Thorne, unpublished, Chapter 3), we also investigated PMO binding affinity for albumin, the most abundant protein in CSF, using microscale thermophoresis (MST). MST is a technique capable of measuring binding interactions by detecting changes in fluorescent intensity upon application of a temperature gradient. We were unable to quantify an equilibrium dissociation constant (K_d) for a PMO-albumin interaction due to negligibly low percentages of bound PMO even at the highest tested albumin concentration, 350 µM (data not shown). Negligible PMO binding to albumin by microscale thermophoresis is in agreement with previous results reporting low protein binding of PMO antisense oligonucleotides. [22]

Discussion

This study resulted in several important findings for PMOs directly administered into the CSF intrathecally in anesthetized rats: (i) PMOs are capable of penetrating superficial brain tissue directly adjacent to the CSF-contacting pial surface by a mechanism that appears consistent with prior measurements of diffusive transport at this interface[9] (Wilken-Resman and Thorne, unpublished, Chapter 3) (ii) PMOs robustly access the perivascular spaces surrounding blood vessels of varying type and caliber, and (iii) PMOs appear to undergo significant clearance from the brain along olfactory pathways across the cribriform plate, with subsequent drainage to regional peripheral lymph nodes in the neck.

The specific carboxyfluorescein-labeled PMO conjugate utilized for our study demonstrated a prominent concentration gradient at the ventral brain surface, suggesting that the

physicochemical properties of the PMO, including the phosphorodiamidate internucleoside linkages and morpholine ring chemical modifications as well as the nucleotide sequence chosen, did not prohibit PMO diffusion from the subarachnoid space CSF across the pial surface. This finding is significant because the pia and the underlying astrocyte endfeet at the surface of the parenchyma (glia limitans) can in some circumstances act as a barrier to the entry of certain substances into the brain.[27] For example, this pial brain surface / glia limitans interface has previously been shown to provide substantial restriction to the surface diffusion of a phosphorothioate-modified antisense oligonucleotide (Wilken-Resman and Thorne, unpublished, Chapter 3). The dorsal pial surface showed dramatically reduced diffusive signal compared to the ventral surface. This is an expected result that has also been demonstrated with other antisense oligonucleotides (Wilken-Resman and Thorne, unpublished, Chapter 3), as well as with proteins following intrathecal administration and is thought to reflect substantially lower dorsal brain surface exposure to subarachnoid CSF, as was demonstrated using MRI following intrathecal infusion of gadolinium labeled IgG. [9]

This study demonstrated a perivascular distribution of PMOs following intrathecal administration using *ex vivo* fluorescence and confocal microscopy. To our knowledge, this is the first study that has identified a PMO antisense oligonucleotide in the PVS, following our recent identification of PS-ASO and 2'MOE-ASO in the PVS of arterioles, venules, and microvessels (Wilken-Resman and Thorne, unpublished, Chapter 3). Confocal imaging at high magnification allowed the visualization of perivascular PMO associated with both arterioles and putative venules and extending down the vascular tree to the microvessel level. aligning with the conception of the PVS as a fluid compartment surrounding vessels of all type and caliber and

potentially allowing for a ‘circulation’ involving inflow via the PVS of arteries and arterioles and outflow via the PVS of venules and veins. [19]

Examination of coronal brain sections demonstrated that PMO perivascular signal was found not only in the cortex, but also in certain subcortical brain regions such as the caudoputamen and the posterior hippocampus, although there was variation in the extent of perivascular delivery to these regions among animals. Given the inefficiency of diffusion over long distances, rapid perivascular delivery of the PMO to subcortical brain structures is an important feature for treating many neurological disorders, including the caudoputamen for Huntington’s disease. [28] The perivascular distribution and surface diffusion seen after intrathecal administration of the PMO appears qualitatively similar to the distribution of a 2’MOE-ASO of the same nucleotide sequence (Wilken-Resman and Thorne, unpublished). Formation of secondary structure for this sequence is unfavorable at physiological temperature, therefore the PMO is expected to occupy space condensed as a random coil. [29,30] Sizing the PMO using integrative optical imaging confirmed the similarity in apparent hydrodynamic diameter between the two oligonucleotides despite differences in chemical modifications and fluorophore (PMO: 3.15 ± 0.07 nm; 2’MOE-ASO: 3.09 ± 0.07 nm) (Wilken-Resman and Thorne, unpublished). This compacted conformation is likely to contribute to enhanced CNS distribution compared to an oligonucleotide with a sequence that supports the formation of a secondary structure. Although it is not possible to make a direct quantitative comparison between the PMO and the 2’MOE-ASO since they are conjugated to different fluorophores, the apparent similarity in their perivascular distribution profiles supports the notion that the sequence-dependent hydrodynamic size of an ASO is an important factor that may be predictive of its perivascular transport in the CNS.

Previous electron microscopy work in cats and rats has shown the existence of pores underlaid by dense collagen fibers located on the lining cells of leptomeningeal blood vessels in the subarachnoid space and that these pores could potentially act as a size-dependent entry site to the PVS. [9,31]

An interesting observation based on the comparison of the distribution of the PMO and the 2'MOE-ASO with identical sequences is that the differences in charge between the PMO, which contained a neutral phosphorodiamidate backbone, and the 2'MOE-ASO, which contained a negatively charged mixed phosphodiester and phosphorothioate backbone, did not appear to translate into a noticeable difference in perivascular access or surface diffusion. It was previously suggested that a charged macromolecule, such as an antisense oligonucleotide with a polyanionic backbone, might experience hindered diffusion in the extracellular space[32] or restricted access to the perivascular smooth muscle basement membrane from the vascular connective tissue space as a result of electrostatic interactions with abundant proteoglycans with fixed negative charge. [14] If this were the case it might be expected that the neutral PMO would demonstrate increased perivascular distribution or surface diffusion compared to the 2'MOE-ASO, a result which did not appear to have occurred with these initial PMO studies. One potential explanation is that the 2'MOE-ASO was small enough that its random interactions with negatively charged components in the extracellular environment were not sufficient to produce a noticeable decrease in distribution compared to the neutral PMO. Furthermore, the physiological salt concentration present in the CSF and interstitial fluid (approximately 150 mM Na)[33] could result in charge screening, effectively limiting the radius of electrostatic effects, or the Debye length, of the ASOs with a charged backbone. [34] Substantial decrease in Debye length could lead to similar

distributions for the small 2'MOE-ASO and PMO despite the nominal difference in backbone charge. The effect of protein binding was not addressed in this comparison because neither the present study nor prior work showed albumin binding to be consequential for the PMO or 2'MOE-ASO, respectively. Further research will be important for understanding how electrostatic interactions and protein binding impact perivascular and diffusive transport of antisense oligonucleotides after intrathecal administration.

The classical understanding of CSF clearance is absorption into the dural venous sinuses via arachnoid villi or granulations. [35] Clearance via cranial and spinal nerves[9] has also been demonstrated, as well as an olfactory pathway for CSF drainage comprised of drainage via perivascular spaces, olfactory nerves, and/or lymphatics across the cribriform plate and to the nasal passages, where they can drain via lymphatics to regional lymph nodes in the neck. [9,36] Drainage of CSF and CSF-borne macromolecules is a topic that has received renewed interest within the last several years with much of the recent discussion focusing on CSF drainage via dural lymphatics. [37,38] While we did not carefully examine dural lymphatics, we did take particular care to examine the olfactory clearance route, which was recently challenged in favor of dural lymphatic clearance. [37] Our findings demonstrate consistent PMO presence in the olfactory nerve layer, cribriform plate, olfactory mucosa, and deep cervical lymph nodes after intrathecal administration, lending further support to the idea that CSF and macromolecules in the CSF drain, at least in part, along rodent olfactory pathways connecting the olfactory subarachnoid space and the lamina propria of the olfactory mucosa (ethmoturbinates of the rat). An obvious caveat is that the olfactory drainage route may differ in relative importance among species and may be more pronounced in rodents than in humans. [39] A better understanding of

charged and uncharged ASO clearance mechanisms following their intrathecal delivery awaits further study.

Taken together, our results establish for the first time that an intrathecal infusion of a PMO can result in robust distribution to perivascular spaces surrounding blood vessels of all type and caliber and a prominent diffusion gradient at the CSF-facing pial surface. The biodistribution of the carboxyfluorescein-PMO conjugate used in this study appeared qualitatively similar to that obtained for a 2'MOE-ASO of the same nucleotide sequence (Wilken-Resman and Thorne, unpublished, Chapter 3), suggesting that ASO hydrodynamic size, as opposed to charge, may be a more important factor for ASO distribution into brain from the CSF. While the lack of an obvious effect for charge (electrostatic interactions) in ASO distribution was not entirely expected, this may be a consequence of the small hydrodynamic size of the PMO used here, along with the substantial charge screening that is a characteristic of physiological salt concentrations in the CSF and ISF (~150 mM NaCl). We also observed prominent PMO clearance from the CNS along olfactory drainage pathways. Gaining a more complete understanding of transport pathways important for CNS distribution and clearance of ASOs will likely contribute to the development of therapeutics optimized for delivery to target cortical and subcortical regions of the CNS.

1. Aartsma-Rus A, Krieg AM. FDA Approves Eteplirsen for Duchenne Muscular Dystrophy: The Next Chapter in the Eteplirsen Saga. *Nucleic Acid Ther*. 2017;27(1):1-3. doi:10.1089/nat.2016.0657

2. Keam SJ. Inotersen: First Global Approval. *Drugs*. 2018;78(13):1371-1376. doi:10.1007/s40265-018-0968-5

3. Scoles DR, Minikel E V., Pulst SM. Antisense oligonucleotides: A primer. *Neurol Genet*. 2019;5(2). doi:10.1212/NXG.0000000000000323

4. Bennett CF. Therapeutic Antisense Oligonucleotides Are Coming of Age. *Annu Rev Med*. 2019;70(1):307-321. doi:10.1146/annurev-med-041217-010829

5. Mathew V, Wang AK. Inotersen: New promise for the treatment of hereditary transthyretin amyloidosis. *Drug Des Devel Ther*. 2019;13:1515-1525. doi:10.2147/DDDT.S162913

6. Geary RS, Norris D, Yu R, Bennett CF. Pharmacokinetics, biodistribution and cell uptake of antisense oligonucleotides. *Adv Drug Deliv Rev*. 2015;87:46-51. doi:10.1016/j.addr.2015.01.008

7. Agrawal S, Temsamani J, Tang JY. Pharmacokinetics, biodistribution, and stability of oligodeoxynucleotide phosphorothioates in mice. *Proc Natl Acad Sci U S A*. 1991;88(17):7595-7599. doi:10.1073/pnas.88.17.7595

8. Khorkova O, Wahlestedt C. Oligonucleotide therapies for disorders of the nervous system. *Nat Biotechnol*. 2017;35(3):249-263. doi:10.1038/nbt.3784

9. Pizzo ME, Wolak DJ, Kumar NN, et al. Intrathecal antibody distribution in the rat brain: surface diffusion, perivascular transport and osmotic enhancement of delivery. *J Physiol*. 2018;596(3):445-475. doi:10.1113/JP275105

10. Wolak DJ, Thorne RG. Diffusion of macromolecules in the brain: Implications for drug delivery. *Mol Pharm*. 2013;10(5):1492-1504. doi:10.1021/mp300495e

11. Papisov MI, Belov V V., Gannon KS. Physiology of the intrathecal bolus: The leptomeningeal route for macromolecule and particle delivery to CNS. *Mol Pharm*. 2013;10(5):1522-1532. doi:10.1021/mp300474m

12. Thorne RG, Nicholson C. In vivo diffusion analysis with quantum dots and dextrans predicts the width of brain extracellular space. *Proc Natl Acad Sci U S A*. 2006;103(14):5567-5572. doi:10.1073/pnas.0509425103

13. Fenstermacher JD, Patlak CS. The movements of water and solutes in brains of mammals. In: Pappius HM, Feindel W, eds. *Dynamics of Brain Edema*. Springer Nature; 1976:88-94.

14. Novak U, Kaye AH. Extracellular matrix and the brain: Components and function. *J Clin Neurosci*. 2000;7(4):280-290. doi:10.1054/jocn.1999.0212

15. Wolak DJ, Pizzo ME, Thorne RG. Probing the extracellular diffusion of antibodies in brain using in vivo integrative optical imaging and ex vivo fluorescence imaging. *J Control Release*. 2015;197:78-86. doi:10.1016/j.jconrel.2014.10.034

16. Cserr H, Cooper DN, Milhorat TH. Flow of Cerebral Interstitial Fluid as Indicated by the Removal of Extracellular Markers from Rat Caudate Nucleus. *Exp Eye Res*. 1977;25:461-473.

17. Rennels ML, Gregory TF, Blaumanis OR, Fujimoto K, Grady PA. Evidence for a “Paravascular” fluid circulation in the mammalian central nervous system, provided by the rapid distribution of tracer protein throughout the brain from the subarachnoid space. *Brain Res*. 1985;326(1):47-63.

doi:10.1016/0006-8993(85)91383-6

18. Abbott NJ. Evidence for bulk flow of brain interstitial fluid: Significance for physiology and pathology. *Neurochem Int*. 2004;45(4):545-552. doi:10.1016/j.neuint.2003.11.006

19. Abbott NJ, Pizzo ME, Preston JE, Janigro D, Thorne RG. The role of brain barriers in fluid movement in the CNS: is there a 'glymphatic' system? *Acta Neuropathol*. 2018;135(3):387-407. doi:10.1007/s00401-018-1812-4

20. Iliff JJ, Wang M, Liao Y, et al. A paravascular pathway facilitates CSF flow through the brain parenchyma and the clearance of interstitial solutes, including amyloid β. *Sci Transl Med*. 2012;4(147):147ra111-147ra111. doi:10.1126/scitranslmed.3003748

21. Amantana A, Iversen PL. Pharmacokinetics and biodistribution of phosphorodiamidatemorpholino antisense oligomers. *Curr Opin Pharmacol*. 2005;5(5):500-555.

22. Sazani P, Magee T, Charleston J, et al. In Vitro Pharmacokinetic Evaluation of Eteplirsen, SRP-4045, and SRP-4053; Three Phosphorodiamidate Morpholino Oligomers (PMO) for the Treatment of Patients with Duchenne Muscular Dystrophy (DMD) (P5.061). *Neurology*. 2015;84.

23. Davson H, Segal MB. *Physiology of the CSF and Blood-Brain Barriers*. Boca Raton: CRC Press; 1996.

24. Yang L, Kress BT, Weber HJ, et al. Evaluating glymphatic pathway function utilizing clinically relevant intrathecal infusion of CSF tracer. *J Transl Med*. 2013;11(1):107. doi:10.1186/1479-5876-11-107

25. Nicholson C, Tao L. Hindered diffusion of high molecular weight compounds in brain extracellular microenvironment measured with integrative optical imaging. *Biophys J*. 1993;65(6):2277-2290. doi:10.1016/S0006-3495(93)81324-9

26. Thorne RG, Hrabetová S, Nicholson C. Diffusion of epidermal growth factor in rat brain extracellular space measured by integrative optical imaging. *J Neurophysiol*. 2004;92(6):3471-3481. doi:10.1152/jn.00352.2004

27. Ghersi-Egea JF, Finnegan W, Chen JL, Fenstermacher JD. Rapid distribution of intraventricularly administered sucrose into cerebrospinal fluid cisterns via subarachnoid velae in rat. *Neuroscience*. 1996;75(4):1271-1288. doi:10.1016/0306-4522(96)00281-3

28. Vonsattel J-P, Myers RH, Stevens TJ, Ferrante RJ, Bird ED, Richardson EP. Neuropathological Classification of Huntington's Disease. *J Neuropathol Exp Neurol*. 1985;44(6):559-577. doi:10.1097/00005072-198511000-00003

29. Roth E, Glick Azaria A, Girshevitz O, Bitler A, Garini Y. Measuring the Conformation and Persistence Length of Single-Stranded DNA Using a DNA Origami Structure. *Nano Lett*. 2018;18(11):6703-6709. doi:10.1021/acs.nanolett.8b02093

30. Goddard NL, Bonnet G, Krichevsky O, Libchaber A. Sequence dependent rigidity of single stranded DNA. *Phys Rev Lett*. 2000;85(11):2400-2403. doi:10.1103/PhysRevLett.85.2400

31. Zervas NT, Liszczak TM, Mayberg MR, Black PM. Cerebrospinal fluid may nourish cerebral vessels through pathways in the adventitia that may be analogous to systemic vasa vasorum. *J Neurosurg*. 1982;56(4):475-481. doi:10.3171/jns.1982.56.4.0475

32. Wolak DJ, Thorne RG. Diffusion of macromolecules in the brain: Implications for drug delivery. *Mol Pharm*. 2013;10(5):1492-1504. doi:10.1021/mp300495e

33. Somjen GG. *Ions in the Brain: Normal Function, Seizures, and Stroke*. New York: Oxford University Press; 2004.

34. Hille B. *Ion Channels of Excitable Membranes*. Sunderland, Massachusetts: Sinauer Associates, Inc; 2001.

35. McComb JG. Recent research into the nature of cerebrospinal fluid formation and absorption. *J Neurosurg*. 1983;59(3):369-383. doi:10.3171/jns.1983.59.3.0369

36. Koh L, Zakharov A, Johnston M. Integration of the subarachnoid space and lymphatics: Is it time to embrace a new concept of cerebrospinal fluid absorption? *Cerebrospinal Fluid Res*. 2005;2:33-38. doi:10.1186/1743-8454-2-6

37. Louveau A, Smirnov I, Keyes TJ, et al. Structural and functional features of central nervous system lymphatic vessels. *Nature*. 2015;523(7560):337-341. doi:10.1038/nature14432

38. Aspelund A, Antila S, Proulx ST, et al. A dural lymphatic vascular system that drains brain interstitial fluid and macromolecules. *J Exp Med*. 2015;212(7):991-999. doi:10.1084/jem.20142290

39. Kida S, Pantazis A, Weller RO. CSF drains directly from the subarachnoid space into nasal lymphatics in the rat. Anatomy, histology and immunological significance. *Neuropathol Appl Neurobiol*. 1993;19(6):480-488. doi:10.1111/j.1365-2990.1993.tb00476.x

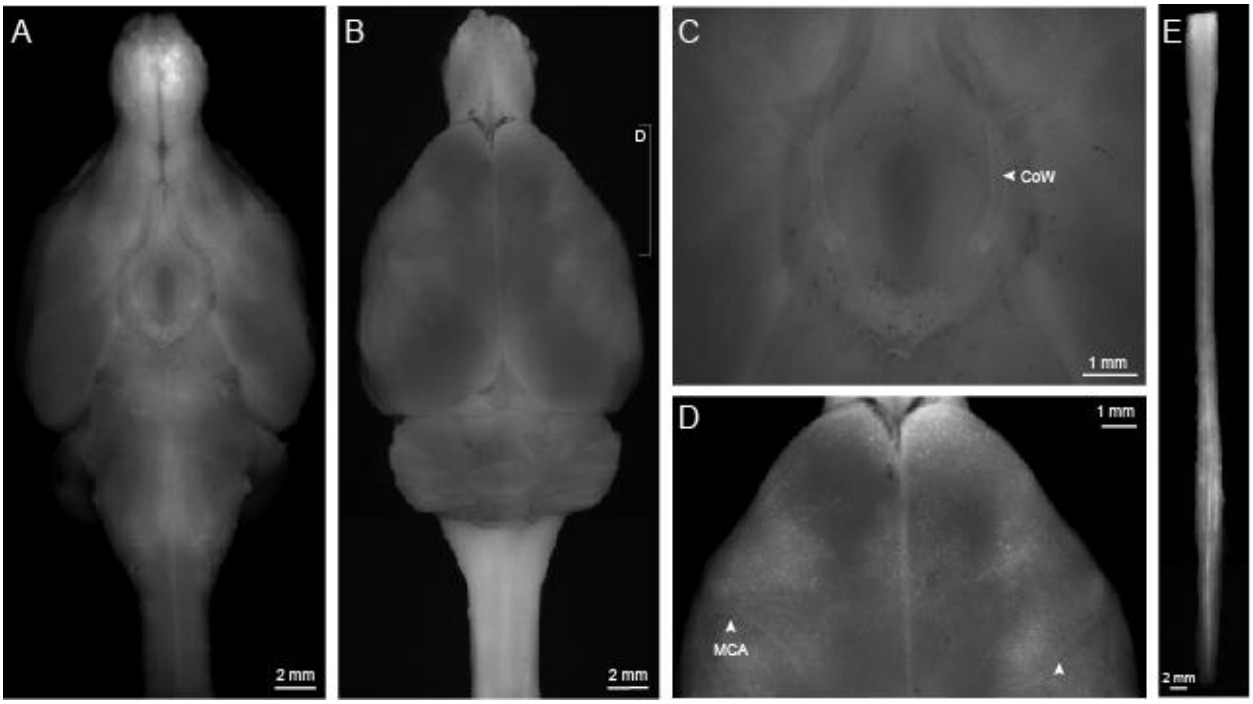

Figure 1: PMO signal at the brain and spinal cord surfaces imaged using *ex vivo* fluorescence microscopy. Ventral (A) and dorsal (B) brain surfaces displayed diffuse fluorescent signal. Signal is also located in the perivascular spaces of large surface vessels including the Circle of Willis (C) on the ventral surface and the middle cerebral arteries on the left and right sides of the dorsal surface, marked with arrowheads (D). Punctate signal resulting from vessels descending perpendicularly into the brain tissue on the ventral surface can also be seen (D). The ventral spinal cord (E) also displayed diffuse PMO signal and signal in the perivascular space of the anterior spinal artery along the length of the spinal cord.

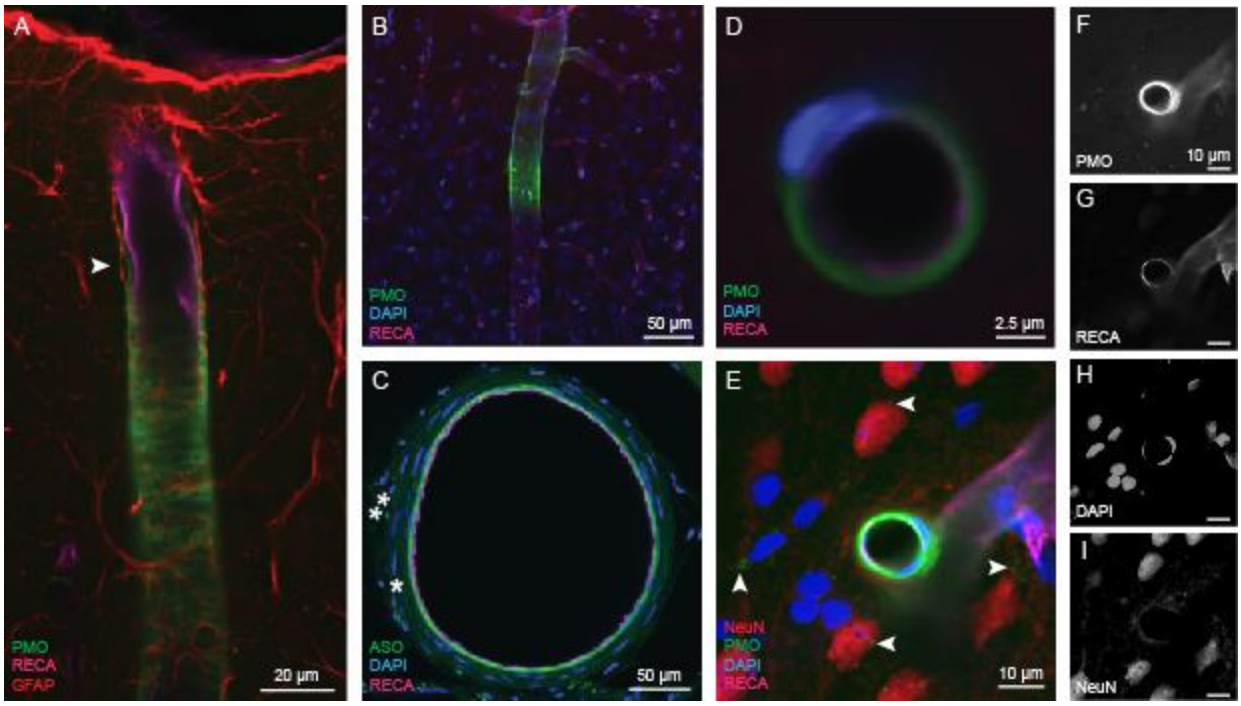

Figure 2: Confocal imaging demonstrated that the PMO distributes to the perivascular space surrounding blood vessels of all caliber after intrathecal infusion. PMO is shown located in the perivascular compartment between the astrocyte endfeet bordering the parenchyma and the endothelial cells lining the lumen of a penetrating arteriole (A). PMO signal is also associated with putative venules (B). A vessel cross-section of the internal carotid artery (C) displayed PMO signal in the smooth muscle basement membrane (*) and the vascular connective tissue space (**). Signal was also shown in small caliber blood vessels, including microvessels (D). Punctate signal is visible near a small vessel containing perivascular PMO and is seen colocalizing with NeuN (E). Arrowheads point to the most visible puncta. F-I: Single channel images corresponding to (E).

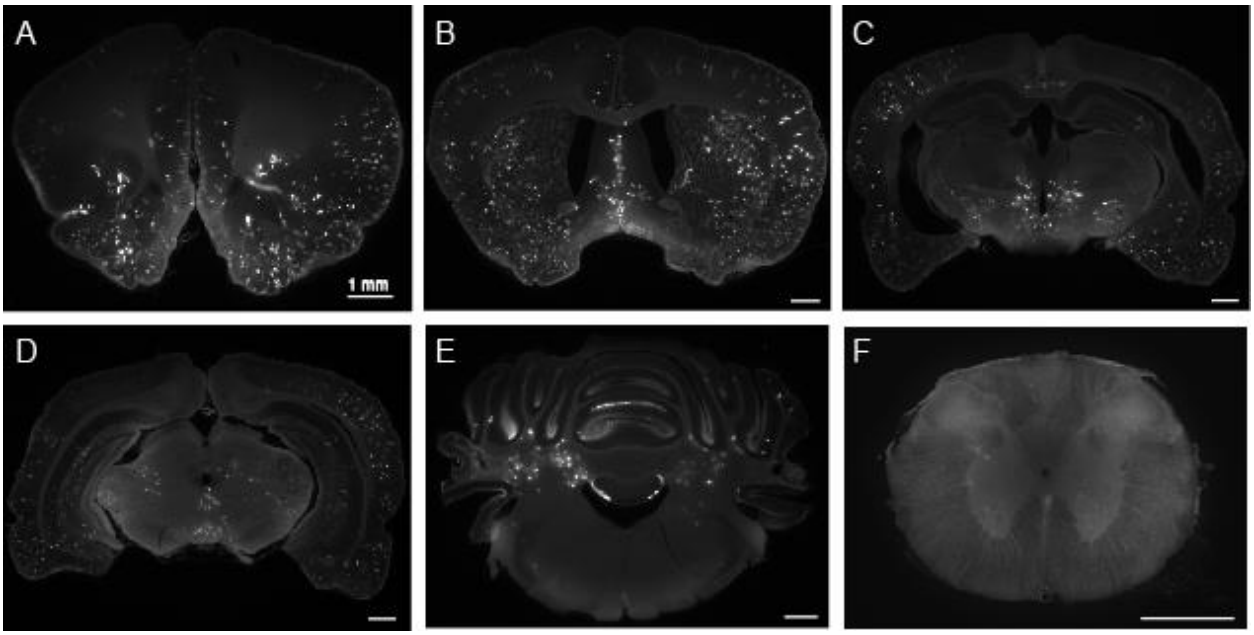

Figure 3: PMO perivascular distribution and diffusion from the pial surface in representative coronal sections from anterior to posterior (A-F). Approximate distance from bregma for each image: (A) +3 mm (B) +1 mm (C) -4 mm (D) -6 mm (E) -10.5 mm (D) cervical spinal cord. Scale bars represent 1 mm.

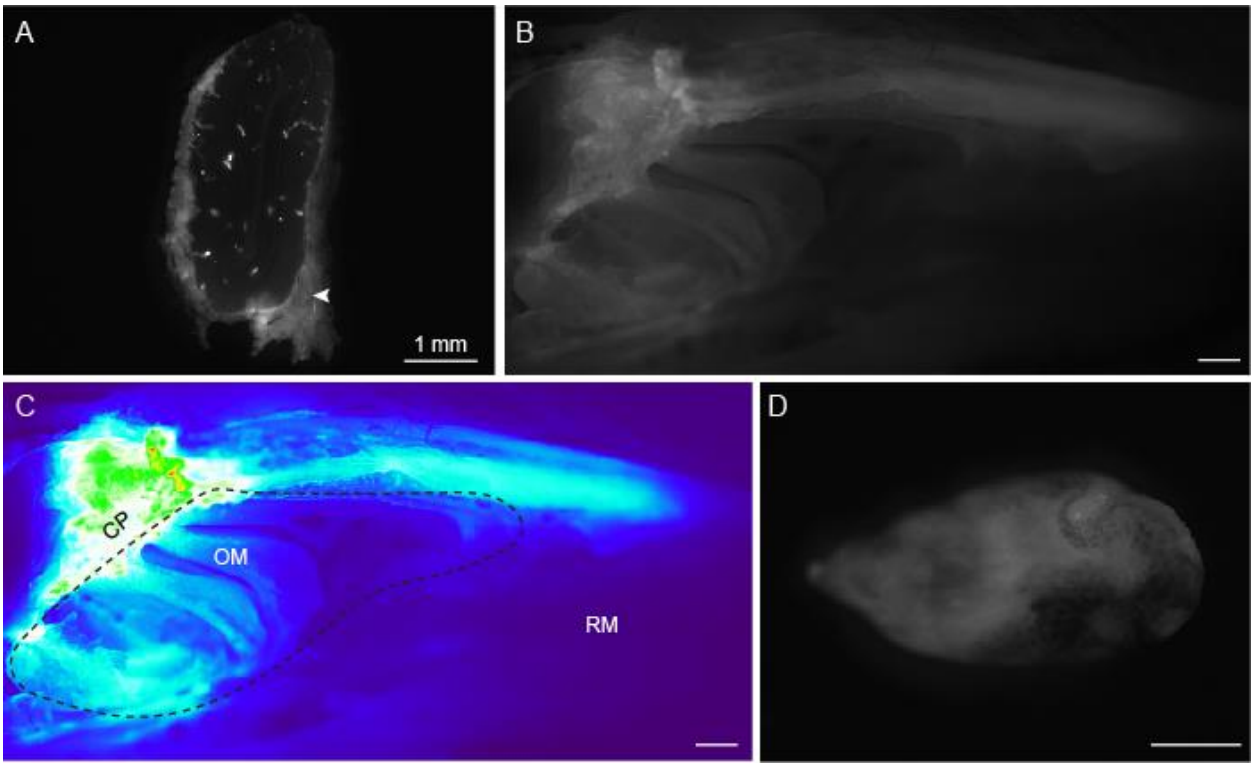

Figure 4: PMO signal was found in regions associated with drainage via an olfactory pathway. (A) Signal in the olfactory nerve layer surrounding the olfactory bulb. The nasal passages shown in (B) and (C, fluorescence intensity map) demonstrated signal within the cribriform plate (CP) and the olfactory mucosa (OM), while little to no signal was associated with the respiratory mucosa (RM). PMO drains to the deep cervical lymph nodes in the neck (D). Scale bars represent 1 mm.

EPILOGUE

Brynna Wilken-Resman

The studies contained in this dissertation represent the first comprehensive examination of the CNS biodistribution of multiple antisense oligonucleotide (ASO) therapeutics following intrathecal administration and the key transport mechanisms that govern this distribution. The fluorophore-labeled ASOs examined herein, a phosphorothioate ASO (PS-ASO), a 2'O-methoxy ethyl ASO (2'MOE-ASO) gapmer, and a phosphorodiamidate morpholino oligonucleotide (PMO), were chosen because they represent the most common ASO chemical modifications currently used in patients (see Chapter 2) and because we hypothesized that subtle differences in their relative size, charge, and binding might result in differences in their effective CNS distribution following infusion into the CSF. This is precisely what the work in this thesis has revealed. These studies have led to several key findings for intrathecally-administered ASOs: i) ASO signal corresponding to transport at CSF-brain interfaces is consistent with diffusive transport based on prior tracer studies[1], ii) rapid transport to CNS tissues—cortical and subcortical—occurs via distribution along perivascular spaces surrounding blood vessels of all type and caliber but the extent to which perivascular distribution occurs differs in a sequence- and chemical modification-specific manner, iii) ASOs with an oligonucleotide sequence that did not support the formation of secondary structure and therefore occupied space as a compacted random coil had a significantly smaller hydrodynamic size compared with a sequence that did form a secondary structure and smaller size correlated with more extensive diffusion and perivascular access.

Our initial work was notable for its focus on characterizing ASO distribution via the perivascular spaces of cerebral vessels, a topic that had been largely ignored in the ASO scientific community up to that point. Several of our findings were surprising or unexpected. The first ASO that we

examined was a fully phosphorothioated ASO with a sequence that was chosen in part because it lacks mammalian targets. This initial PS-ASO work demonstrated very limited diffusion and perivascular access to the brain from the CSF compartment. This limited distribution contrasted with the clinical use and demonstrated efficacy of certain intrathecally-administered ASOs, which suggested that there might be sequence- or chemical modification- specificity associated with CNS biodistribution of ASOs, although no prior literature existed to suggest that this might be the case. We therefore conducted the next phase of our studies with an ASO that was more relevant to those in clinical use. For this purpose, we chose RG6042 (formerly known as HTT_{RX}), the ASO currently in Phase 3 clinical trials for Huntington's disease, and designed a commercially purchasable ASO that closely mimicked RG6042, based on public information contained within a HTT_{RX} patent filing (and published in a paper detailing results from Phase 1/2 clinical trials.) [2] We found that intrathecal administration of this ASO, referred to as the '2'MOE-ASO' within this dissertation, resulted in significantly increased perivascular distribution and a stronger diffusion gradient at the pial surface. The dramatic difference in the CNS distribution of these two ASOs was unexpected. This new result and the discussion it generated inspired us to explore the factors that led to this difference. One interesting finding was our discovery of significant PS-ASO binding interactions with animal-derived CSF and, later, with known CSF concentrations of albumin. The PS-ASO-albumin binding significantly increased the mean apparent size of the ASO, a finding that was surprising since the presence of CSF proteins is often considered negligible. We have speculated that the larger PS-ASO-protein complex interferes in some way with the ability of this complex to diffuse into brain across the pial surface and to access the perivascular spaces of most cerebral blood vessels, with the result being a dramatically blunted and diminished CNS biodistribution from the CSF compartment.

More work is clearly needed to identify other factors that might be at play but our findings are notable for identifying an important, previously unrecognized biodistribution parameter for ASOs (CSF protein binding) that can be easily screened for in academic or private sector drug development settings.

After examining the effects of size, charge, and CSF protein binding between the non-targeted PS-ASO and the 2'MOE-ASO surrogate for RG6042 (see Chapter 3), we decided to next examine a phosphorodiamidate morpholino oligonucleotide (PMO) ASO analog to more explicitly probe the effect of charge on CNS biodistribution. PMOs are a type of ASO where the anionic internucleoside linkages normally present in an ASO (typically phosphodiester or phosphorothioate) are replaced with uncharged phosphorodiamidate linkages. PMOs therefore lack the negative charge inherent in native DNA and most ASO chemical modifications; importantly, PMOs have also previously been shown to exhibit low protein binding similar to the 2'MOE-ASO class of ASO (Chapter 4). We therefore designed a PMO to consist of the same nucleotide sequence as the 2'MOE-ASO so that we could focus specifically on the effects of charge. We expected that the PMO might have increased CNS distribution due to the absence or reduced capacity for electrostatic interactions or protein binding. Contrary to our expectations, we found that the PMO distribution after intrathecal administration looked qualitatively similar to that of the 2'MOE-ASO. While this reinforced our hypothesis that the small hydrodynamic size of the PMO and 2'MOE-ASO, which occupy space as compacted random coils due to their oligonucleotide sequence, is likely important for their extensive CNS distribution following intracisternal infusion, it suggested that the effects of charge may be less prominent than previously thought (see Chapter 4 for a more detailed analysis). It is important to note that the

comparison between the 2'MOE-ASO and PMO was imperfect due to differences in the fluorophore label employed. The fluorophore conjugated to the 5' end of the PS-ASO and 2'MOE-ASO was AlexaFluor488 while the fluorophore conjugated to the 5' end of the PMO was carboxyfluorescein. Every effort was made to match the fluorophores, but commercial manufacturer limitations unfortunately did not allow use of an AlexaFluor488 label for the PMO conjugate. The AlexaFluor488 was our preferred fluorophore, as it has been shown to have minimal effect on protein binding. [3] However, it is possible that the fluorophore choice may not have significantly altered the distribution, e.g. neither the AlexaFluor488 nor the carboxyfluorescein labels comprised more than 10 % of the molecular weight of the ASO used for our studies (Chapters 3 and 4). We suggest that our results for the PMO and the 2'MOE-ASO may in fact illustrate pronounced and substantial charge screening of these molecules at physiological extracellular salt concentration (specifically the approximately 150 mM Na content of CSF and interstitial fluid) such that these small ASOs distribute similarly. If true, this also represents an important finding with possibly broad implications for other ASOs that might be used for CNS applications.

Although this research and its findings represent an advance for our understanding of CNS distribution and transport mechanisms following intrathecal administration of ASOs with different sequences and chemical modifications, there is of course much work remaining. Future work that may be important for further advancements include the use of two-photon or three-photon[4] imaging for an enhanced understanding of temporal aspects of ASO perivascular distribution and high-throughput binding studies such as the recently developed fluorescence polarization assay[3] which may be adapted for studying interactions of differing ASO chemistries

with major constituents of the extracellular matrix and CSF. Together with continued studies examining the *in vivo* CNS distribution of ASOs with varying sequence, chemical modifications, and perhaps also a range of different fluorophore labels, these studies will likely be able to more precisely define the optimal characteristics of ASOs to achieve a more efficient distribution to target brain and spinal cord regions.

Finally, in addition to further research examining single-stranded ASOs, there is an opportunity to expand this research to include other oligonucleotide therapeutics such as siRNA (double stranded RNA). Preliminary results suggest that siRNA may distribute more favorably than ASOs in brain tissue, based on *in vivo* biodistribution data examining tortuosity, or diffusional hindrance in the outermost neocortex of anesthetized rats (Figure 1). 2018 marked the first FDA approval of an siRNA therapeutic (patisiran). [5] Although patisiran is not a CNS therapeutic, there is growing interest in using intrathecal siRNA to treat neurological disorders. [6]

Based on current FDA approvals for oligonucleotide therapies and their extensive appearance in clinical trials (Chapter 2), it is expected that further successes will follow in the future and that novel ASO and siRNA drugs will ultimately prove to be highly impactful therapies for disorders in the periphery and the CNS. Biodistribution and transport studies such as those contained in this thesis may provide the basis for a stronger conceptual framework for understanding ASO and siRNA delivery focused on biological targets in the brain and spinal cord. It is our hope that such work will assist in developing these therapies for optimal CNS distribution and efficacy to reduce the burden and impact of a number of devastating neurological conditions.

1. Pizzo ME, Wolak DJ, Kumar NN, et al. Intrathecal antibody distribution in the rat brain: surface diffusion, perivascular transport and osmotic enhancement of delivery. *J Physiol*. 2018;596(3):445-475. doi:10.1113/JP275105

2. Tabrizi SJ, Leavitt BR, Landwehrmeyer GB, et al. Targeting Huntingtin Expression in Patients with Huntington's Disease. *N Engl J Med*. 2019:NEJMoa1900907. doi:10.1056/NEJMoa1900907

3. Gaus HJ, Gupta R, Chappell AE, Østergaard ME, Swayze EE, Seth PP. Characterization of the interactions of chemically-modified therapeutic nucleic acids with plasma proteins using a fluorescence polarization assay. *Nucleic Acids Res*. 2018;47(3):1110-1122. doi:10.1093/nar/gky1260

4. Wang T, Ouzounov DG, Wu C, et al. Three-photon imaging of mouse brain structure and function through the intact skull. *Nat Methods*. 2018;15(10):789-792. doi:10.1038/s41592-018-0115-y

5. Mullard A. FDA approves landmark RNAi drug. *Nat Rev Drug Discov*. 2018;17(9):613-613. doi:10.1038/nrd.2018.152

6. Setten RL, Rossi JJ, Han S ping. The current state and future directions of RNAi-based therapeutics. *Nat Rev Drug Discov*. 2019;18(June):421-446. doi:10.1038/s41573-019-0017-4

7. Wolak DJ, Thorne RG. Diffusion of macromolecules in the brain: Implications for drug delivery. *Mol Pharm*. 2013;10(5):1492-1504. doi:10.1021/mp300495e

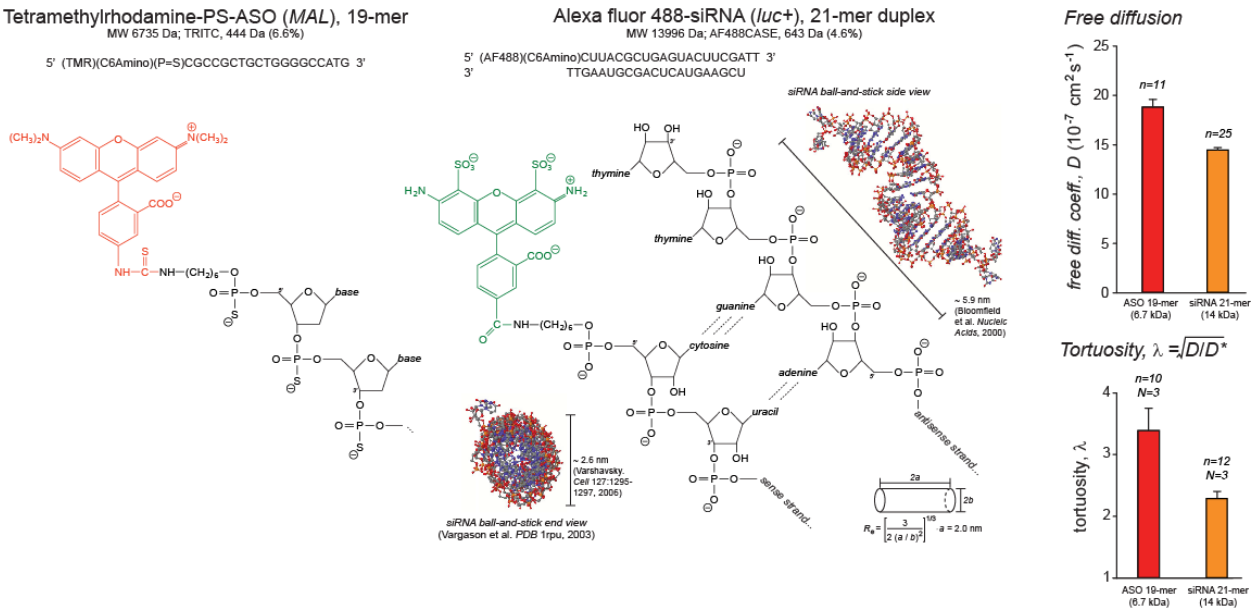

Figure 1: Free diffusion coefficients and tortuosity of representative ASO and siRNA oligonucleotides. Tortuosity is a measure of diffusional hindrance that takes diffusion in agarose (free diffusion, *D*) and diffusion in brain (*D**) into account. [7] The siRNA is larger than the ASO, as indicated by its larger molecular weight and reduced free diffusion coefficient. However, preliminary results indicate that the ASO exhibits a larger tortuosity, meaning that it experiences more hindrance to diffusion in the brain extracellular space compared to the siRNA. Further research could examine sources of this difference in tortuosity and its relevance in CNS distribution overall. Figure adapted from earlier data obtained with the method of integrative optical imaging *in vivo* in anesthetized rat somatosensory cortex (Thorne et al, *Unpublished*).